ANNALS OF GEOPHYSICS, 67, 4, S430, 2024; doi:10.4401/ag-9154
OPEN ACCESS

Precision Seismicity of the San Andreas Fault System in Central California: Insights into Active Tectonics and Earthquake Physics

William L. Ellsworth*,[1]

(1) Stanford University, Department of Geophysics, Stanford, California, USA

Article history: received September 16, 2024; accepted September 27, 2024

Abstract

Since the late 1960s, seismicity of the San Andreas Fault system in central California has been under intense observation by U. S. Geological Survey's Northern California Seismic Network (NCSN). Designed to provide accurate focal depth control and a low magnitude of catalog completeness, the network maps fault, both large and small across the full breadth of this 400-kilometer-long portion of the plate boundary, including many that are known only from their seismicity. Beginning in 1984, with the advent of routine digital recording, new opportunities were created to significantly enhance the spatial resolution of seismicity. This led to the co-evolution of method that take full advantage of digital waveforms and new insights into the nature of seismicity and faults. Collectively referred to as precision seismicity, discoveries included repeating earthquakes and highly organized and stable distributions of seismicity on major faults. Long term observation of seismicity before and after the six largest earthquakes over the last half-century underscore the outstanding challenges for earthquake predictability and theories of earthquake nucleation.

Keywords: Seismicity; Active Faults; Foreshocks; Earthquake Nucleation

1. Introduction

How do we "see" into the Earth? Geology and geophysics have long worked in tandem to infer the structures, materials and forces that control active geologic processes. For most methods, the deeper we look the fuzzier and less certain our knowledge becomes, either due to uncertain extrapolation of surface measurements, or the loss of spatial resolution inherent in many geophysical imaging methods. Reflection seismology is an exception, at least in the sedimentary section, but has had limited success in the crystalline crust or complex geology.

Today, earthquake catalogs routinely contain tens of thousands to hundreds of thousands of events. Although the information per event is limited, typically a position in space locating either where rupture initiated (hypocenter) or the center of the rupture (hypocentroid), magnitude, time of occurrence and perhaps a focal mechanism, collectively they reveal the complex geometry of faults and their evolution in both space and time when the location is sufficiently accurate. The goal of precision seismology is to resolve fault zone structures at scales comparable to earthquake source dimensions of the smallest events considered.

In this paper, I focus on the insights into tectonic and the earthquake source along the San Andreas Fault system in central California derived from four decades of high precision locations from the Northern California Seismic Network (NCSN) (Fig. 1). The base catalog for this work is the double-Difference catalog of Waldhauser and Schaff (2008), with updates through the end of 2021 and real-time additions to the present time. Earthquake hypocenters in their catalog have typical uncertainties of 10s of meters or less. Similarly precise catalogs are now being routinely produced by seismologists throughout the world using a collection of methods that will be referred to as "precision seismicity". Earthquake hypocenters obtained through these methods reveal geometry and movement of seismically active faults with outcrop precision from the top to bottom of the seismogenic crust.

Following a review of the earthquake location problem, a few key examples illustrating the power of precision seismicity for identifying repeating earthquakes and revealing fault zone structure are presented. The nearly 40 years of precision seismicity together with the longer-term catalog of the NCSN long-term are then used to examine the evolution of seismicity in the source region of the region's six M 6-class earthquakes since 1969.

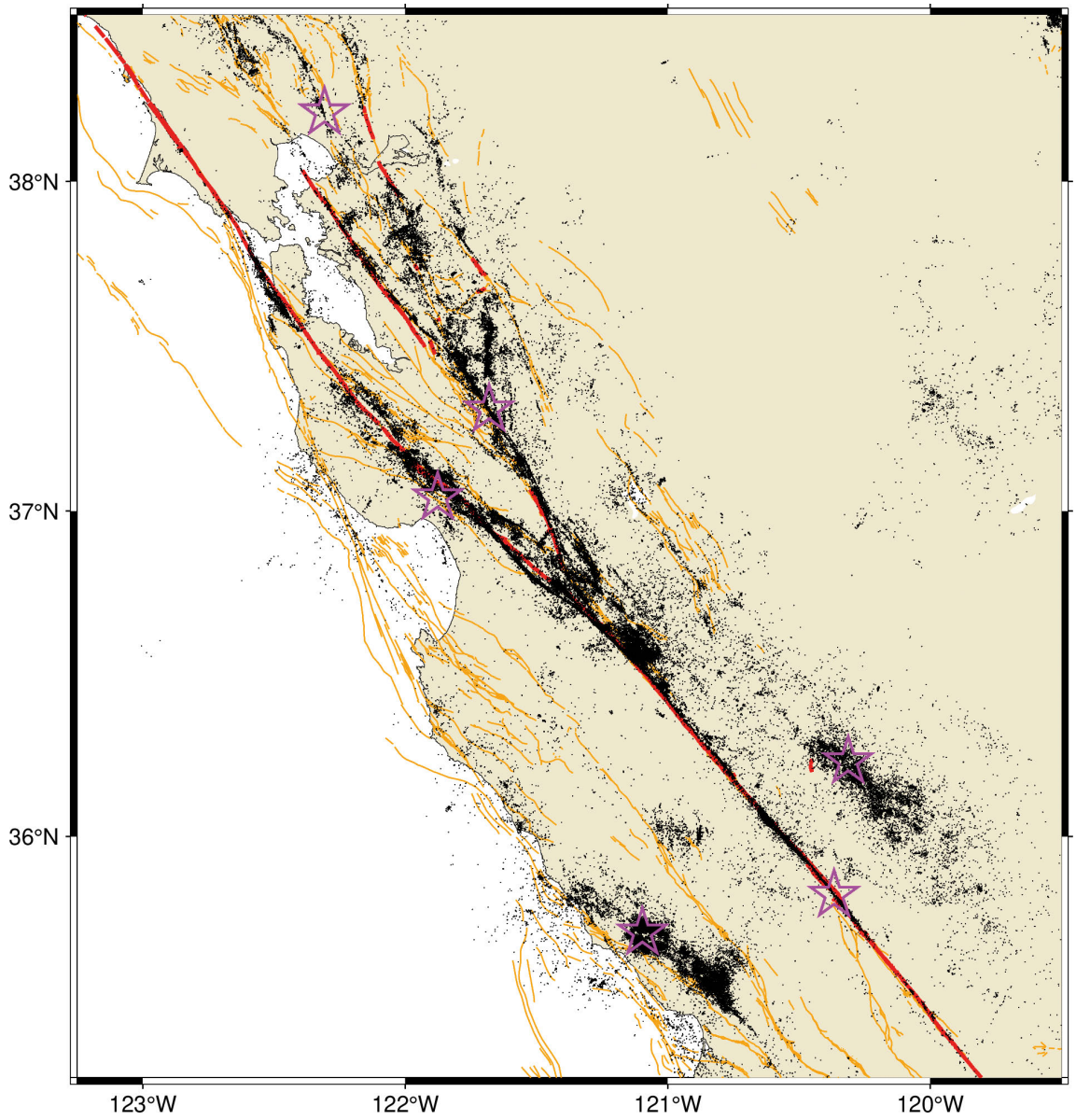

Figure 1. Map of seismicity and active faults in the Central California region. Historic fault ruptures in red, Holocene faults in orange. Double difference earthquake catalog of Waldhauser and Schaff (2008 updated) from 1984 through 2021 shown as points. Stars identify epicenters of the six $M \geq 6$ earthquakes since 1969. From south to north: M_W 6.5 2003 San Simeon, M_W 6.0 2004 Parkfield, M_W 6.7 1983 Coalinga, M_W 7.0 1989 Loma Prieta, M_W 6.2 1984 Morgan Hill and M_W 6.0 2014 South Napa earthquakes.

2. A Brief History of the Precision Hypocenter Problem

At the most basic level, the analysis of most earthquakes consists of just a handful of simple measures extracted from the complex wave train in the seismogram. Arrival times of body waves are used to locate the event and wave amplitudes give a quantitative measure of earthquake size. The resulting earthquake catalogs generally contain the coordinates of the event (latitude, longitude and focal depth), along with a scalar measure of size (magnitude or seismic moment) and possibly the faulting mechanism (fault plane solution or moment tensor), but rarely more. Despite the limited information content per event, when viewed jointly, they reveal a wealth of information about the geometry and temporal evolution of activated faults from which much can be learned about in situ conditions and material properties.

There are, of course, hundreds of studies that contributed new ideas and algorithms for solving the hypocenter program over a span of many decades. In the interest of space, I have restricted this discussion to a few among many that influenced my thinking over the past 50 years.

The modern era of local earthquake seismology got underway the late 1960's with the deployment of dense instrumental networks of continuously recording seismic stations. Among the earliest was the USGS telemetered short period seismic stations along the San Andreas Fault system in central California (Eaton et al., 1970a). Stations were deployed with an interstation distance of approximately 10 to15 km to ensure that focal depth could be routinely determined. To manage the greatly increased volume of routinely detected earthquakes, computer programs for locating the events, determining their magnitudes and focal mechanisms were needed. One of the earliest comprehensive programs was HYPOLAYR, written by Eaton (1966) to handle the analysis of the 1966 Parkfield earthquake aftershocks (Eaton et al., 1970b). Anyone who plans to write a computer program to locate earthquake should study this paper. Among other advances, it used multiple crustal models instead of a table for travel time and partial derivative calculations and tuned station corrections to account for the strong crustal structure contrast across the San Andreas Fault.

The rapid growth of the Northern California Seismic Network (CalNet, now NCSN) necessitated the updating of the hypocenter program to handle routine processing, including importantly outlier detection and removal with program HYPO71 (Lee and Lahr, 1975). Further developments including programs HYPOELLIPSE (Lahr, 1989) and HYPOINVERSE (Klein, 2002; n.b. references are to recent updates). These three programs, along with many others that followed are widely used today.

The main factors limiting location accuracy (where the hypocenter really is in the Earth) and precision (the uncertainty of the location in the frame of the velocity model) typically include the measurement accuracy of wave arrivals, azimuthal gaps in the station coverage, lack of a near station, and differences between the assumed and true velocity model. On small scales, precision can be improved using one of many available joint hypocenter methods, in which the travel time discrepancy between the model and individual station is factored out of the problem. See Pujol (1988) for a discussion of methods. This procedure works well on small scales but fails as the dimension of the source region grows. So, one might ask what is small enough or too large a volume?

As an important first step would be to have a simple yet accurate crustal velocity model for use in single event hypocenter programs. Wesson (1971) had shown that earthquake travel time data could be used to recover crustal structure in the presence of strong lateral velocity contrasts. Crosson (1976) linearized problem to solve for hypocenters, a plane layered velocity model and station terms using local travel time data. Steve Roecker and I were working on this problem at the same time at MIT, developing joint hypocenter 3-dimensional structure inversions (Roecker, 1982). That effort grew over the years with important contributions from Robert Nowack, Edi Kissling, Urs Kradolfer and Hans-Rudi Mauer to eventually became VELEST (Kissling et al., 1994, 1995). This approach worked well, even in areas with strong lateral contrasts as encountered by Eaton et al. (1970b) by estimating multiple layered models but could not be extended to large distances due to variability of crustal structure. Either large-scale 3D tomographic models solving the fully coupled hypocenter-structure problem (Thurber, 1983) would be required, or another approach would be needed.

Accuracy of the arrival time measurements is as important as that of the model travel time for achieving precision hypocenters. At first look, it might appear impossible to measure travel times to greater accuracy than the sample rate of the data, particularly when the frequency content of the seismogram is much lower than the Nyquist frequency. But when the seismograms for a pair of events are similar enough, the relative travel time difference between them can be measured with sub-sample precision, either directly in the frequency domain by measuring the slip of the phase of the cross spectrum (Nakamura, 1978; Poupinet et al., 1984) or by interpolation in the time domain (Deichmann

and Garcia-Fernandez, 1992). While both the frequency and time domain measurements are effective, my personal preference is to measure the time difference in the frequency domain, where the frequency-by-frequency values of the coherency guides the selection of frequencies to include in the measurement. The time shift is proportional to the linear slope of the phase spectrum, a one parameter linear problem. When measuring the differential arrival time between pairs of events for either the P or S wave, it is possible to make subsample measurements even when the first arrival (where a time pick is usually made) is uncertain. Since the differential measurement refers to the wave packet, which is typically longer than the actual duration of the earthquake source, the measurements correspond to the earthquake centroid rather than the point of initial rupture. Locations made with such measurements are the hypocentroid of the event, or geometric center of slip. This becomes important when comparing one event to another – did they rupture the same area on the fault or are just nearby to each other?

The need to determine precise hypocenters over large distances while taking full advantage of subsample timing motivated the development of the double difference algorithm. Poupinet et al. (1984) used VELEST to show that a pair of microearthquakes along the Calaveras Fault in California were repeating earthquakes, the first so identified with precision. A significant step in direction of extending to more events and a large spatial domain was made by Got et al. (1994) who implemented a version of the double difference equations for highly coherent events in the east rift zone of Kilauea Volcano, Hawaii. The method was freed from the constraint of selecting a master event but required correlated events to be added in stages, while continuing to refine the locations of the full set of events. It utilized high-precision differential travel times measured with subsample precision in the frequency domain (Poupinet et al., 1984). With this algorithm they produced spectacular results, focusing the scattered standard hypocenter locations onto a narrow fault plane: the detachment fault of the south flank of Kilauea Volcano. Dodge et al. (1995, 1996) used a similar approach to relocate foreshocks, but mixed both arrival time and cross correlation time data, thus accommodating both similar and distinct mechanisms in the same solution. Both studies worked over linear dimensions of 2 to 3 km.

Motivated by the potential for imaging the internal structure of faults, Rubin et al. (1999) analyzed a 30-km-long segment of the San Andreas Fault in central California in the transition from the creeping to locked fault. They adapted the algorithm of Got et al. (1994) to relocate 65 multiplets along the fault, approximately ¾ of the events in the NCSN catalog on this section of the fault. The results revealed the tight clustering of seismicity in horizontal (slip vector parallel) streaks, transforming our understanding of seismicity on this major plate boundary fault. Working independently and at the same time, Waldhauser and Ellsworth (2000) developed a new double-difference algorithm, hypoDD, to efficiently "determine high-resolution hypocenter locations over large distances". The algorithm incorporated both arrival time readings and differential travel times and placed no restriction on event similarity. Applied to the Hayward Fault beneath Berkeley, California, they also found the seismicity to be organized in slip parallel streaks (Waldhauser et al., 1999).

The scale over which the algorithm can be applied is today limited only by the computer resources. Over 900,000 events are contained in the double difference catalogs for all northern California covering 1984-2021 (Waldhauser and Schaff, 2008), and in the 2016-2017 Central Italy sequence catalog of Tan et al. (2021). For the NCSN in northern California, the double difference catalog grows in near real-time, using the base catalog (now covering 1984-2021) to add new events as they occur (Waldhauser, 2009).

Development of such large catalogs has been greatly aided and accelerated by machine learning algorithms for event identification and phase arrival time picking (Mousavi and Beroza, 2022). Together with programs for computing the 10's of millions of differential travel time needed for precision location, analysis of years of continuously recorded data from large networks outperforms analysist-based analysis in every metric (Chiaraluce et al., 2022).

Today, many good alternatives to hypoDD are available, including the programs using source specific station terms of Richards-Dinger and Shearer (2000), Lin and Shearer (2006) and Lomax and Savvaidis (2022). The GrowClust method of hierarchical clustering of Trugman and Shear (2017), and HypoSVI of Smith et al. (2022) using physics informed neural nets represent additional promising directions. Yu et al. (submitted) evaluated the performance of each of these programs, along with several single event location methods, using a realistic synthetic data set based on the 2019 Ridgecrest, California earthquakes. All programs performed reasonably well, although evaluation of location uncertainty, both accuracy and precision, revealed that more work remains to be done with several of the programs. It is also worth noting that despite being called "relative location programs", several including hypoDD achieved sub-kilometer absolute horizontal accuracy in this synthetic test. Focal depth, however, was less well recovered by most programs, with hypoDD the only one with mean precision below 200 m. Consequently, one should always be cautious when interpreting vertical "pipe-like" structures.

In the following sections, several of the key areas where precision seismicity reveals new insights into tectonics and source physics in central California are reviewed. The specific studies discussed, which could easily be replaced by hundreds of others, were chosen to illustrate progress in the development of our understanding.

3. Crustal Architecture of the San Andreas Fault System

Much has been written about the San Andreas Fault system and for those wishing to learn more about the geology, tectonics and seismicity Wallace (1990) is a great place to start. The system in central California contains hundreds of mapped faults, spanning 100 km or more perpendicular to the northwest-trending North America – Pacific plate boundary (Fig. 1). It is loaded at a rate of approximately 40 mm/yr of right later plate motion and produces earthquake of up to approximately M 8 on the major strike slip faults. While some of the major faults are outlined by their recent seismicity, the 1906 rupture segment of the San Andreas Fault has hosted even very few microearthquakes in recent decades (Fig. 1). Seismicity also defines numerous small scale structures off the major faults or in their internal structure (Fig. 2).

The stress field that currently acts of the fault system has the greatest horizontal principal stress oriented nearly perpendicular to the San Andreas and other major faults (Zoback, et al., 1987). This normal loading to the plate

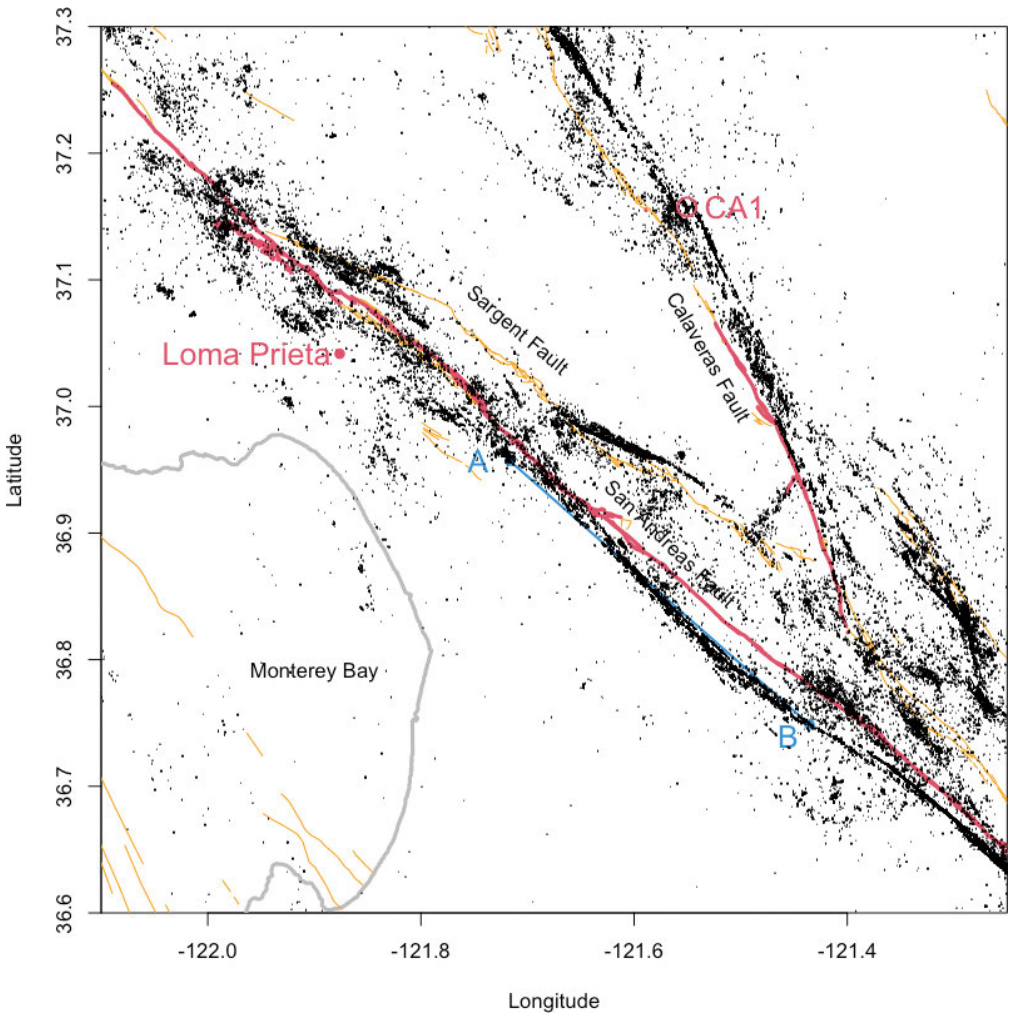

Figure 2. Seismicity of the bifurcation of the San Andreas Fault at the northern end of the creeping section into the northward continuation on the Peninsular San Andreas and Calaveras Faults. Earthquakes and faults shown as in Fig. 1. Epicenter of the 1989 Loma Prieta earthquake shown as red dot. Red circle identifies repeating microearthquake CA1. Endpoints of San Andreas cross section of Fig. 5 at A and A′. Holocene active faults in orange and historical ruptures in red. Pacific coastline in gray.

boundary results in crustal uplift from slip on reverse faults with magnitudes of up to 7. In fact, the three largest earthquakes in the region since the 1906 San Andreas earthquake were on previously unrecognized reverse faults: Coalinga (M_W 6.7) in 1983, Loma Prieta (M_W 7.0) in 1989 and San Simeon (M_W 6.5) in 2003. In contrast, the largest strike slip earthquake over the same period were Morgan Hill (M_W 6.2) in 1984, Parkfield (M_W 6.0) most recently in 2004, and South Napa (M_W 6.0) in 2014. Clearly, identifying and characterizing those hidden faults remains a critical task for hazard assessment in the region (Field, et al., 2014).

Precision seismicity has had a major impact on our understanding of active tectonics by revealing fault structure and architecture at outcrop scall throughout the crust. Today, it is hard to remember that the association between earthquakes and faults was debated until the evidence became overwhelming. The clear association between fault rupture and aftershock seismicity in the 1966 M 6 Parkfield earthquake (Eaton et al., 1970b) helped motivate a fundamental change in how the San Andreas plate boundary was monitored, replacing traditional observatory stations spaced a hundred or more kilometers apart with dense networks.

By the mid-1980s over 500 continuously telemetered seismic stations were in operation by USGS and Caltech, providing end-to-end coverage of the plate boundary (Hill et al., 1990). Both the location and depth extent of active faults were revealed by routine analysis of their activity. As was known from classical network analysis (Hileman et al., 1973), seismicity was spread across a wide region of the plate boundary, but with clear concentrations along some, but not all the major faults. Off fault activity clearly reflected distributed brittle deformation, but the best locations often lacked the resolution to unambiguously define the underlying fault structures. For example, while network coverage of the M_W 6.7 Coalinga earthquake of 1983 provided hundreds of accurate focal mechanisms, the actual rupture plane or planes was difficult to discern with standard location methods (Eaton, 1990; Eberhart-Phillips and Reasenberg, 1990).

4. Repeating Earthquakes

When the methods of precision seismicity were applied to catalog readings and waveforms, new and unexpected features emerged. A number of these were discovered where the central creeping San Andreas splits into the Peninsula segment and Calaveras Fault (Fig. 2). It was here that repeating earthquakes and time-dependent variations in crustal wave velocity were first demonstrated (Poupinet et al., 1984). Previously hidden internal structures within the faults including the tight horizontal alignment of hypocenters were also revealed in the work of Rubin et al. (1999), Waldhauser et al. (1999) and Schaff et al. (2002).

One of the earliest “repeaters” to examined in detail “CA1” was first noted in 1980 in some of the earliest digital data of the NCSN. Finding this event and its subsequent repeats was a needle-int-the-haystack problem when using ordinary catalog data (Fig. 3). Comparison of the upper left map of catalog locations with the double-difference locations in the upper right clearly illustrates the improved resolution of structures obtained by precision locations. The lower left figure reveals the internal complexity of the Calaveras fault in the subsurface, placing CA1 on a small linear fault segment in a compressional step over between fault branches to the south and north. The horizontal precision inferred from the narrowness of the seismicity of approximately 10 m agrees with location uncertainties from hypoDD. High correlation between seismograms provides useful guidance to potential repeats, but proof through precise relocation, demonstrating overlap of the centroids is required to validate recurrence (Ellsworth, 1995). The lower right of Fig. 3 compares the standard NCSN locations with the DD locations with the dot marking the centroid location and circle the radius for source dimension assuming a 3 MPa stress drop.

CA1 source sprang into action as an aftershock of the 1984 Morgan Hill earthquake, following an Omori-like pattern of logarithmically increasing recurrence intervals: 3 in the first 3 days, 7 more in the next 7 months and a total of 19 by the end of 1991 (Vidale et al., 1994). The Waldhauser and Schaff (2021) repeating earthquake catalog documents 7 more through 2012 (Fig. 4). This pattern of lengthening recurrence intervals during the first few years of the extended aftershock sequence, coupled with systematics of the seismic moment and rupture dimension were used by Marone et al. (1995) to infer fault strengthening during the interseismic period. This pattern of increasing moment with log hold time through approximately the first 500 days of the aftershock sequence reversed over the next 30 years as the recurrence intervals stabilized to a relatively constant value (Fig. 4). Reasons for the reversal are not clear, although measurement error is unlikely as the relative moments measured using amplitude correlations have a precision of about 1% (Waldhauser and Schaff, 2021). Variability in the recurrence interval and relative moment of individual repeaters are subject to multiple causes, including potential changes in loading rate on the fault.

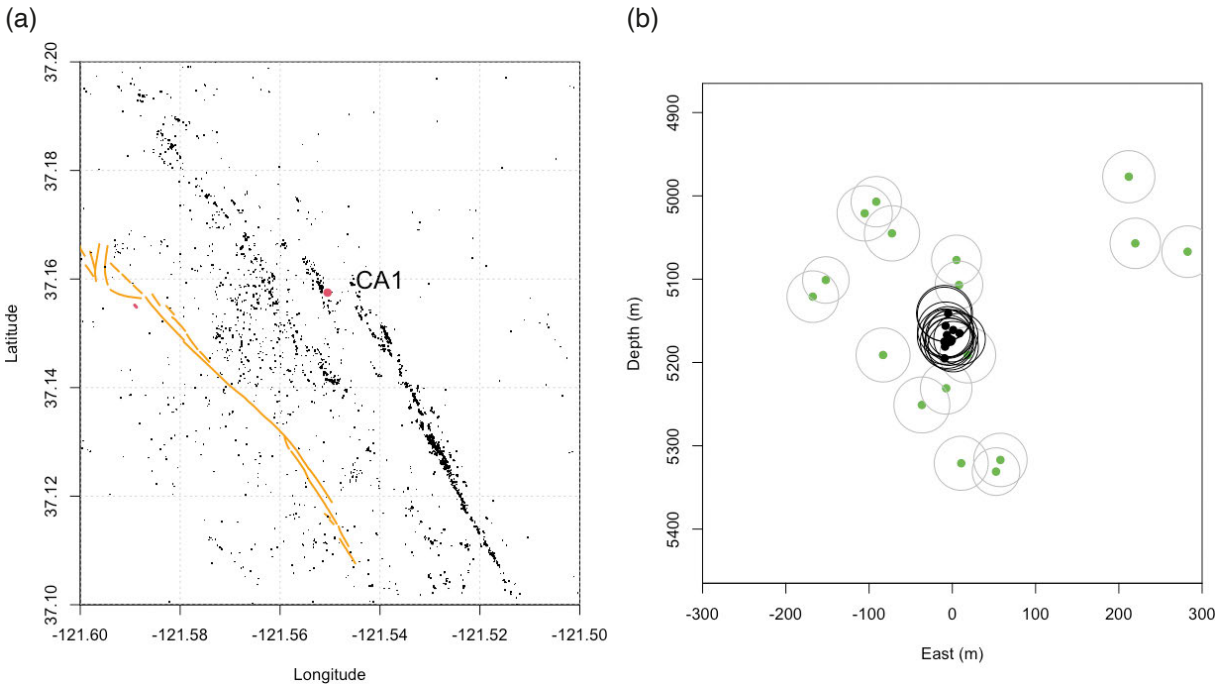

Figure 3. (a) Repeating earthquake CA1 (red dot) located in a left step of the Calaveras Fault. Note the complexity of off fault seismicity at all scales. (b) Fault parallel cross section of CA1 showing hypocentroids (black) and equivalent circular rupture dimension for 3 MPa stress drop from precision relocations of Waldhauser and Schaff (2021) and standard catalog hypocenters (green) and equivalent source dimensions.

Rubinstein et al. (2012) found that a fixed recurrence interval better explained repeating earthquakes in California, Taiwan and Japan than either the time- or slip-predictable model. Future research studying multiple repeating events on short fault segments may lead to a deeper understanding of the controls on recurrence time and magnitude.

5. Streaks of Repeating Earthquakes

Clusters of repeating earthquakes that form rake-parallel streaks provide particularly good targets, as first found on the San Andreas Fault to south of CA1 by Rubin et al. (1999). These events locate on the southernmost part of the 1906 earthquake rupture which terminated in the town of San Juan Bautista (Fig. 2). The segment also includes at its northern end the southernmost 8-12 km of the 1989 Loma Prieta earthquake aftershock zone, as defined by its early aftershocks, where merges seamlessly onto the creeping central segment of the San Andreas Fault (Dietz and Ellsworth, 1990 and 1997). In cross section, repeaters shown as black dots correspond to the 1984-1991 time frame analyzed by Rubin et al. (1999) and in red covering 1992-2014 in Waldhauser and Schaff's catalog (Fig. 5a). Also shown in cross section are the non-repeating earthquakes from the same time period portrayed as circular ruptures for a 3 MPa stress drop. The large event at the northwest (left) end of the section is the M_L 5.4 Chittenden earthquake of April 18, 1990, the largest aftershock of the entire Loma Prieta sequence.

The activity rate along this segment of the fault responded vigorously to the stress change imparted by the Loma Prieta mainshock (Reasenberg and Simpson, 1997). During the aftershock period, the response was stronger closer to the rupture, as expected, and decayed with time. By dividing the segment into three equal pieces of 12 km length and counting the annual number of repeats from all sources in the segment, we can follow the response for a quarter century (Fig. 5b). Recalling that the Loma Prieta earthquake occurred early in the 4^{th} quarter of 1989, the repeater rate jumped the most relative to pre-1989 rates in the northwest section where only 9 repeaters occurred in the 5 years before the earthquake compared with 75 in 1989, or a rate increase of over a factor of 200. To the southeast, the rates increased by factors of about 10 and 5. All zones show an initially declining rate that persisted for a decade or more, far longer than the 2.3 year duration within primary aftershock measured by Reasenberg and Simpson (1997). Similar results for this segment's response to the Loma Prieta earthquake were found by

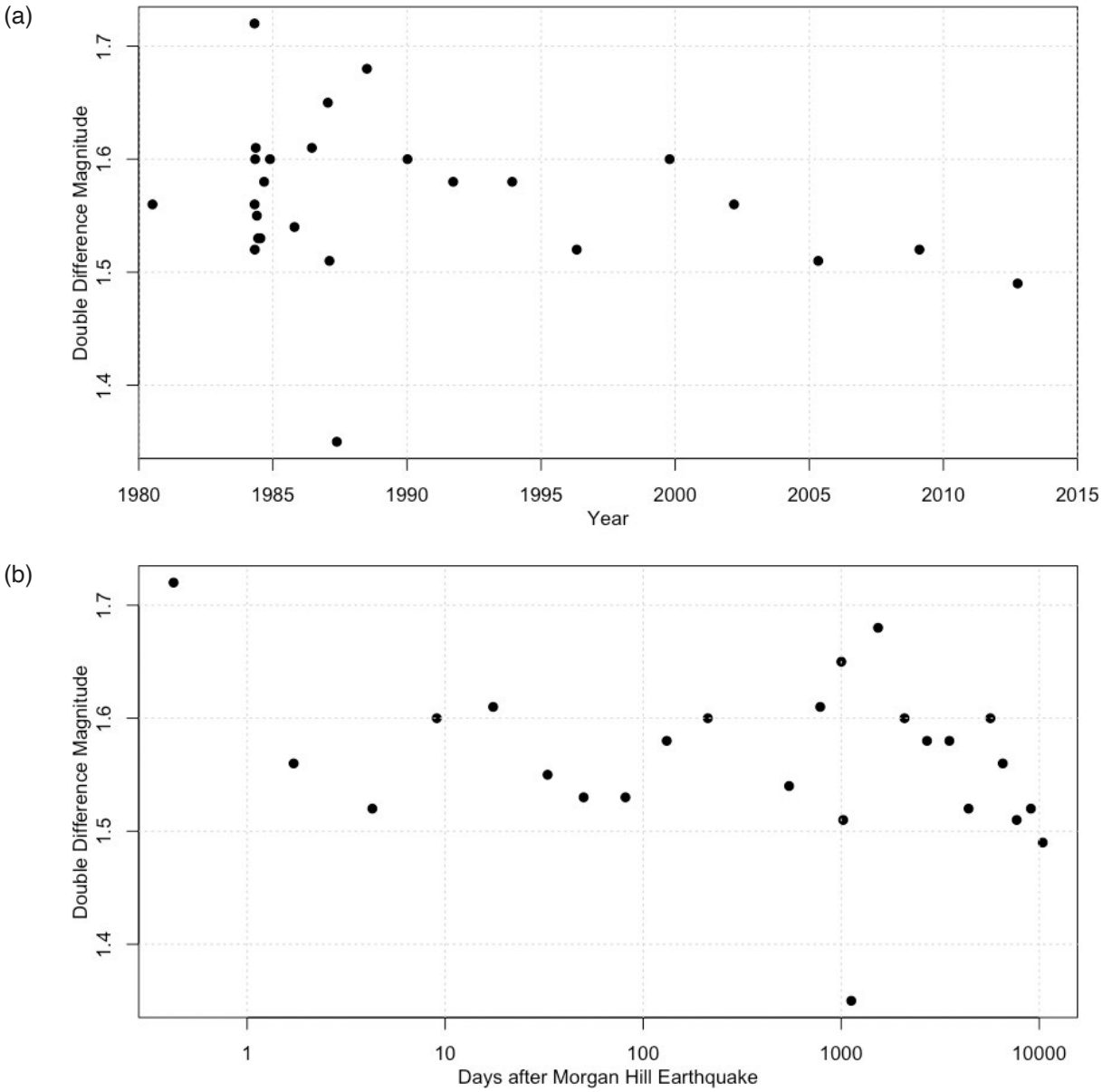

Figure 4. Time series of CA1 earthquakes. (a) Waveform determined magnitude versus calendar time from earliest known member of family in 1980 through end of repeating earthquake catalog of Waldhauser and Schaff (2021) in 2014. Note the dramatic decrease in recurrence interval following the 1984 Morgan Hill Earthquake. (b) Post Morgan Hill recurrences in log time. Comparing the upper and lower figures, a transition from Omori-like recurrence intervals to constant intervals can be identified approximately 1 decade after the Morgan Hill earthquake.

Templeton et al. (2008) who also noted local response to additional earthquakes including the 1998 M 5.1 by tracking variations of recurrence intervals for individual repeater families.

The examples discussed above just skim the surface where repeating earthquakes have been used interrogate the state of the fault at hypocentral depths (e.g. Nadeau and McEvilly, 2004; Uchida and Bürgmann, 2019). In addition, temporal changes in wave velocity discovered by Poupinet et al. (1984) using interferometric analysis of repeating earthquake coda waves has evolved into a powerful method for studying the time dependent response of velocity and attenuation to strong shaking, principally in near surface materials (Schaff and Beroza, 2004; Rubinstein and Beroza, 2004). Recent work by Sheng et al. (2021) went further by using 1-5 Hz coda waves to isolate the velocity changes caused by the M_W 6.0 2004 Parkfield earthquake to shallow depth. Because higher frequency coda waves (10-20 Hz) were insensitive to the velocity change, they suggested that the coda consists of low frequency reverberations amplified by low-velocity near surface materials and high frequency waves scattered from deeper depths. Clearly, much has been learned using repeating earthquakes with great potential for doing much more.

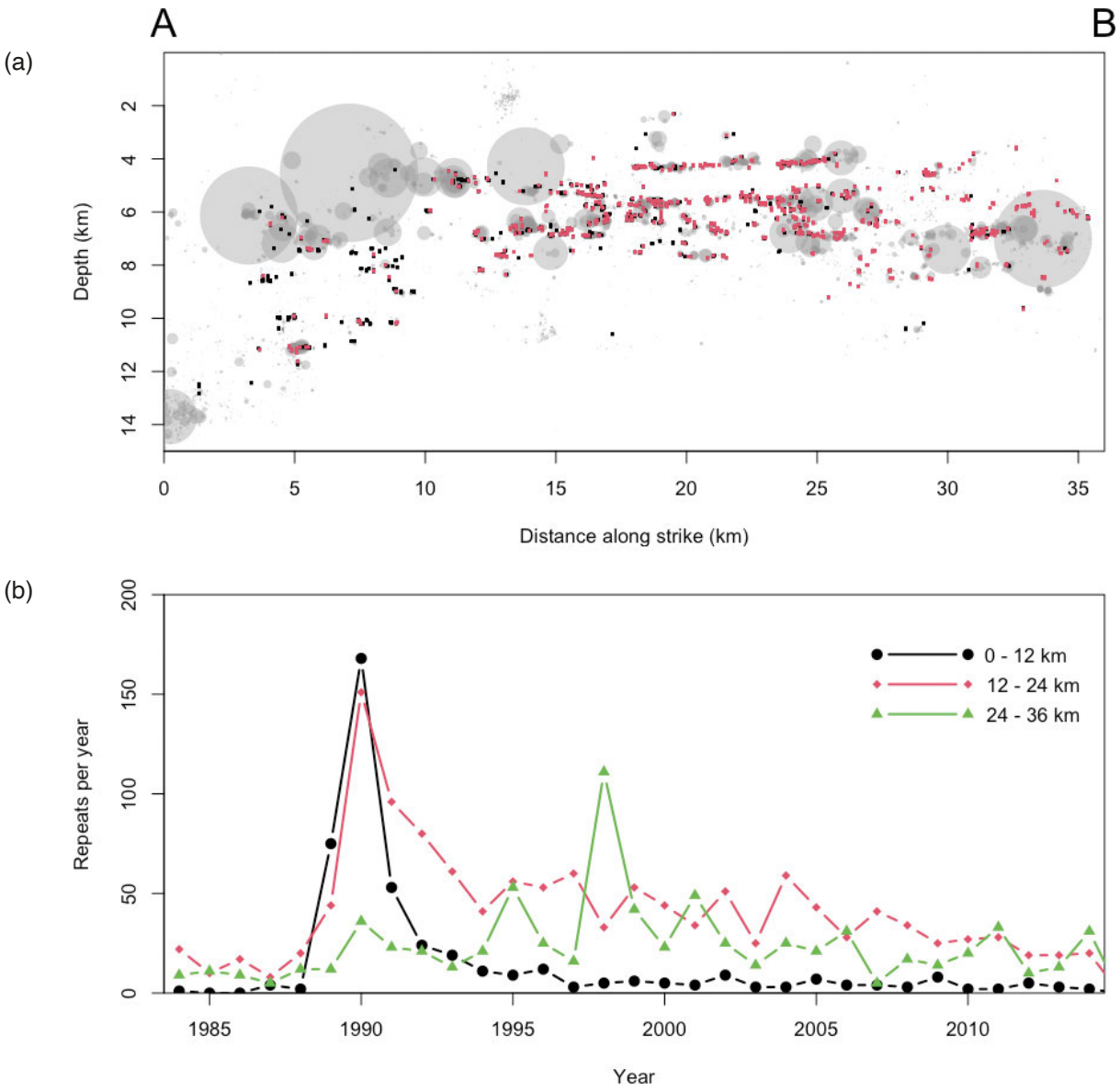

Figure 5. (a) Cross section along the San Andreas Fault in the double difference catalog of Waldhauser and Schaff (2008 updated). Hypocentrioids of repeating earthquake included in Rubin et al. (1999) from 1984-1991 in black and updated from 1992-2021 in red. Rupture areas of non-repeating earthquakes for 3 MPa stress drop shown in gray. The large events at the left end of the cross section are late aftershocks of the 1989 Loma Prieta earthquake. (b) Annual count of repeating earthquakes in three equal sections along the profile. Note the strong response to the Loma Prieta earthquake in both space and time.

6. Seismicity Preceding Large Earthquakes

In this section, the seismic activity associated with the ruptures of the region's six magnitude 6-class earthquakes is briefly examined using the available time span of seismic monitoring. The goal is to bring out what preceding seismicity revealed about the future event.

6.1 M_W 6.7 Coalinga Earthquake of May 2, 1983

The reverse faulting Coaling earthquake ruptured beneath the Coalinga anticline on the east flank of the Central California Coast Ranges (Fig. 1). It occurred 8 months before the end of the era of analog recording and manual

phase reading of the NCSN. The prior to the installation of station PAR in September 1975, at what turned out to be just 3 km from the epicenter, the nearest permanent seismic stations were located 30 km to the southwest along the Parkfield segment of the San Andreas Fault. Consequently, the catalog is heterogeneous with respect to magnitude of completeness and accuracy of locations with time and at no point prior to 1984 would be considered "precision seismicity" in the Coalinga region. A comprehensive reference on the earthquake can be found in Rymer and Ellsworth (1990) which contains extensive analysis of the aftershocks by Eaton (1990) and Eberhart-Phillips and Reasenberg (1990) among other chapters.

Between 1975 and the Coalinga mainshock in 1983 the region around the earthquake was frequently active, both within the principal aftershock zone and on its periphery (Fig. 6). Notable sequences occurred in early 1975 on the southern edge of the aftershock zone (M_{max} 4.9, gray symbols in Fig. 6), within the aftershock zone to the east of the epicenter in 1980 (M_{max} 4.5, green symbols in Fig 6) and 1981 (M_{max} 3.5, blue symbols in Fig. 6), and to the northwest in 1982 (M_{max} 2.9, orange symbols in Fig. 6). However, only minor activity was detected in 1983 before the earthquake. There were also no immediate foreshocks at a detection threshold of M 0. The closest events within 1 month of the event, M_D 1.8 and 1.9, occurred 4 km to the southeast of the epicenter. While there was no short-term runup of activity to the mainshock, when viewed from a decadal perspective, it is clear that the fault system was seismically active. This earthquake had a major impact on seismic hazard evaluation, highlighting the need to identify hidden basement faults, especially those associated with geologically young folds with axes parallel to the plate boundary which may grow principally in large magnitude earthquakes (Stein and Ekström, 1992).

Complicating matters is the possibility that elevated pore pressure contributed to the occurrence of the earthquake, either by natural processes (Yerkes et al., 1990) or possibly related to long-term production from the Coalinga oil field (Segall and Yerkes,1990). The occurrence of two other earthquakes the 1985 M_L 5.6 (now M_W 6.1) Kettleman North Dome and 1987 M_W 5.9 Whittier Narrows earthquakes also beneath major oil fields formed by young anticlinal structures raises questions of causality that continue to be relevant today (McGarr, 1991). Although not examined in detail here, the 1985 mainshock was preceded by significant seismicity in months leading up to the mainshock, including foreshocks as large as M_L 4.7 on the day of the event. This swarm-like buildup to the mainshock

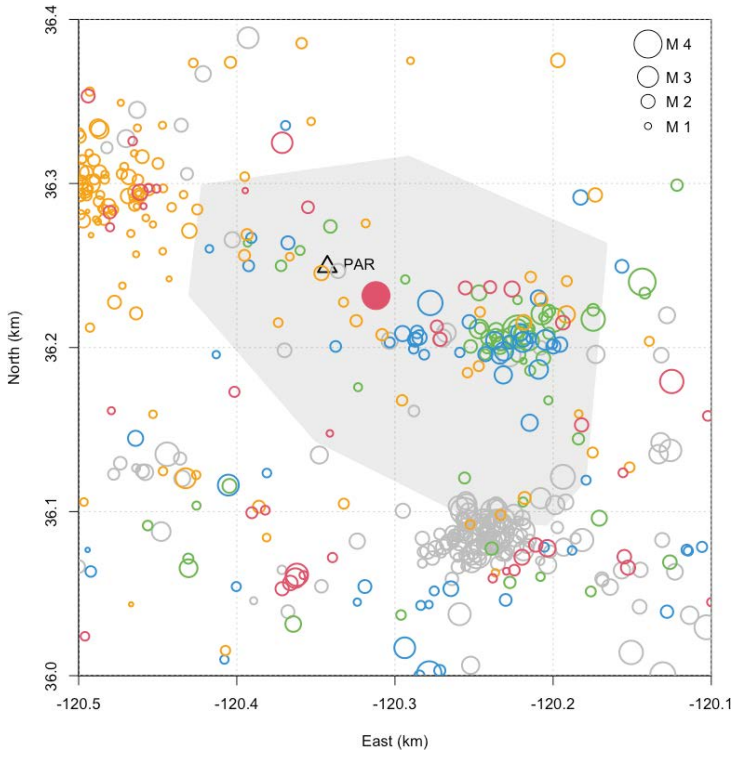

Figure 6. Map of the epicentral area of the M_W 6.7 1983 Coalinga earthquake showing activity before the earthquake. Red dot marks the epicenter of the earthquake. Triangle marks the nearest seismic station. Approximate bounds of the aftershocks in gray. Earthquakes from 1975-1979 in gray, 1980 in green, 1981 in blue, 1982 in orange and 1983 to time of mainshock in red.

is suggestive of fluid involvement, whether natural or not, as seen in many cases of both induced seismicity or swarm activity in the Imperial Valley at the southern end of the San Andreas Fault.

6.2 M_W 6.2 Morgan Hill Earthquake of April 24, 1984

A 25 km-long segment of the Calaveras Fault ruptured unilaterally to the southeast in this right lateral strike slip earthquake (Bakun et al., 1984; Fig. 1). Located within the original core coverage area of the NCSN, earthquakes Mc ~ 1.5 from 1969 to Mc ~ 1.0 by 1980, the earthquake provided an early opportunity to examine the evolution of seismicity preceding a large plate boundary fault earthquake. This segment of the Calaveras Fault was studied by Schaff et al. (2002) whose precision seismicity detailed the highly streaked nature of seismicity along the fault. The along fault cross section from Fig. 2 of Shaff et al. (2002) is reconstructed in Fig. 7 using standard NCSN catalog locations from 1969 to the time of the earthquake (top) and with double-difference locations from Waldhauser and Schaff (2008) through 2021 (bottom). In each panel, the Morgan Hill hypocenter appears as a red symbol. In the upper panel, hypocenters are identified by a point and circular rupture areas for a 3 MPa stress drop are in gray. In the upper panel, only the hypocenters are shown. The large event nearest the hypocenter is the M_L 4.8 earthquake of

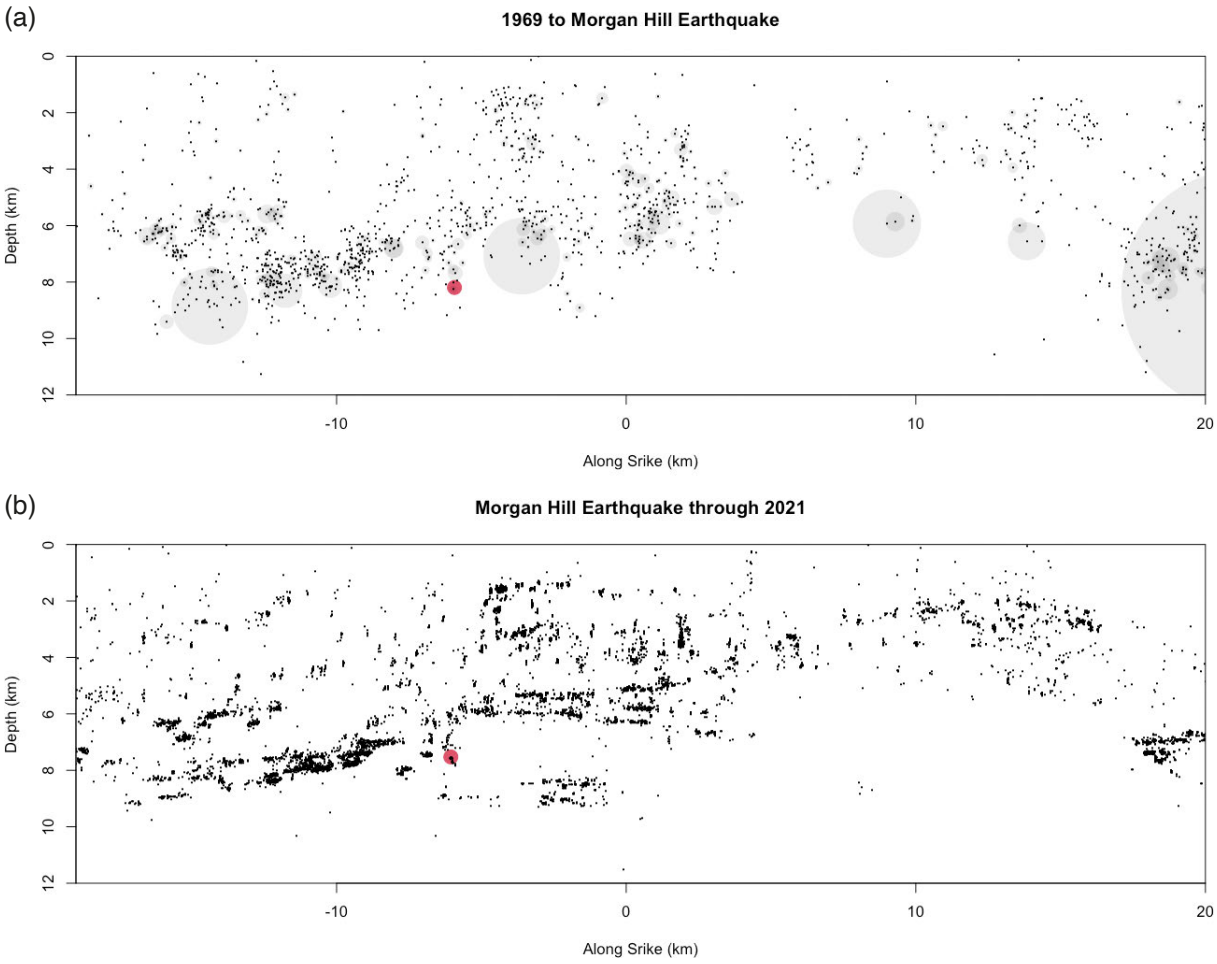

Figure 7. Fault parallel Cross section along the M_W 6.2 1984 Morgan Hill earthquake rupture zone along the Calaveras Fault. (a) Seismicity 1969 to Morgan Hill earthquake from the standard NCSN catalog. Hypocenters shown as points and gray circles correspond to circular rupture area for a stress drop of 3 MPa. Large even at right edge is the M_W 5.7 1979 Coyote Lake earthquake. Mainshock hypocenter in red. (b) Double difference hypocentroids from mainshock through 2021. Vertical elongation of repeating earthquake clusters suggests relative depth resolution of 100-200 m for this catalog. Note that upper panel contains both single event locations (1969-1983) and a few months of double difference locations.

May 8, 1979, and the large event at the right (south) end is the M_W 5.7 Coyote Lake earthquake of August, 6, 1979 (Reasenberg and Ellsworth, 1982).

Although the differences between standard and precision locations is apparent when comparing the two panels, the overall distribution of seismicity seen in high precision can be seen in the pre-Morgan Hill seismicity. Simply put, the same general locations of activity did not change significantly because of coseismic slip or stress redistribution in the earthquake, an observation first made for the 1972 M_L 5.0 Bear Valley earthquake (Ellsworth, 1975). Along faults that both creep and produce small to moderate magnitude earthquakes, the nucleation sites change slowly in response to slip, resulting in numerous repeating earthquakes, such as CA1 discussed above.

Given this static spatial pattern, did the hypocentral region of the Morgan Hill earthquake exhibit any significant changes in seismicity as the earthquake approached in time? The answer is 'no', or at least none that are apparent. Focusing in on the hypocenter (Fig. 8) it is seen that the mainshock hypocenter locates near one small cluster that appears no different than others nearby. The three events closest to the hypocenter occurred in 1973 and 1975, with the larges M_D 2.7. The more energetic cluster about 500 m above hosted a M_L 3.1 event in 1969 and a M_L 3.4 in 1979 and nothing after 1981. Bakun et al. (1984) examined a wide range of potentially precursory phenomena, but found none aside from two foreshocks, M_D 0.7 and 0.4, 18 and 3 hours before, respectively.

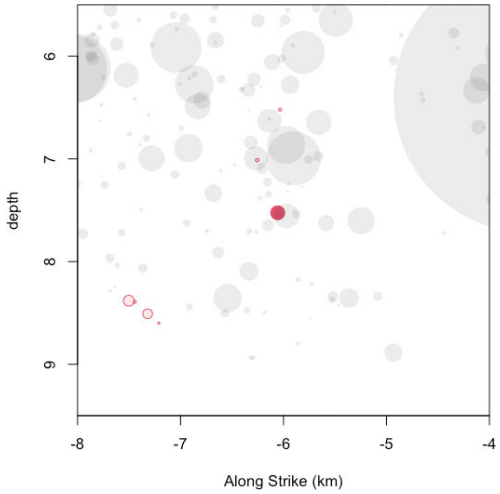

Figure 8. Fault parallel cross section around the hypocenter of the Morgan Hill earthquake (red dot). Seismicity in 1969-1983 shown in gray by circles corresponding to rupture area for 3 MPa stress drop. Preshocks in 1984 shown by red circles with radius for 3 MPa stress drop. The ML 4.8 May 8, 1979 earthquake is the large event on the right side of the section.

6.3 M_W 7.0 Loma Prieta Earthquake of October 18, 1989

The Loma Prieta earthquake (Figs. 1 and 2) is the largest earthquake in the central San Andreas Fault system south of the Mendocino Triple Junction since 1906, causing widespread damage and loss of life in the San Francisco Bay Area. The scientific, engineering and societal findings and lesson from the event have been extensively discussed, including in the multi-volume U.S. Geological Survey Professional Paper on the earthquake (Johnston, 1993; Simpson, 1994; Spudich, 1997; Reasenberg, 1997; Harris, 1998; Wells, 2004). It ruptured blind oblique-reverse fault that as it propagated southward warped into a more vertical dip and merged with the southernmost end of the 1906 rupture of the San Andreas Fault (Dietz and Ellsworth, 1990). The steeply dipping fault plane rises from the hypocenter at 16 km to intersect the San Andreas fault at a depth of 4 km (Dietz and Ellsworth, 1997).

The epicentral area sits within the core monitoring area of the NCSN since August 1967, permitting the detailed examination of preseismic activity and its association with the earthquake. In broad brush, seismicity in the epicentral was sparce in the 2 decades before the earthquake, failing to highlight the eventual rupture plane of the earthquake (Dietz and Ellsworth, 1997 and Fig. 9). Preceding seismicity largely localized at the north end of

the Sargent Fault, including the M_L 5.3 June 27, 1988 and M_L 5.4 August 8, 1989 Lake Elsman earthquakes. Prior to the earthquake, was extensive discussion in the community prior to Loma Prieta about the potential for M 6-7 earthquakes in the San Francisco Bay Area which in some cases included explicit reference to earthquakes in what proved to be the epicentral area (Harris, 1998). None of the forecasts anticipated the actual location, orientation of the fault plane or faulting style, and cannot be rigorously retrospectively tested in according to Harris (1998). Among them the one by Lindh (1983) came closest in identifying the location and length of the earthquake.

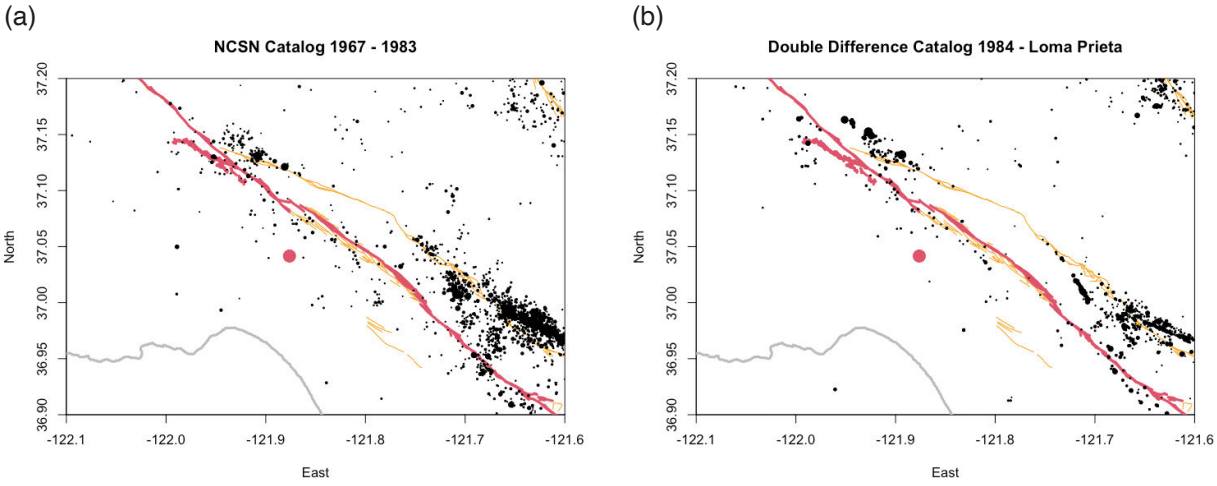

Figure 9. Seismicity preceding the 1989 M_W 7.0 Loma Prieta earthquake. (a) Earthquakes from the NCSN catalog 1969-1983. (b) Double Difference catalog from 1984 to mainshock.

Our interest here is in what these data reveal about seismicity in the vicinity of the hypocenter. In the 22 years before the earthquake, no event was detected with a hypocentral distance of 2 km. The closest was a M_D 1.3 in 1973 at 2.3 km (Ellsworth, 2019). Double Difference seismicity before and after the earthquake viewed in oblique projections (Fig. 10) show not only how vacant the space around the hypocenter was before the earthquake, but afterward as well. This observation is consistent with the arguments for a total stress drop in the event made by Michael et al. (1990) and Beroza and Zoback (1993). What little we can say about the nucleation process of the earthquake is that the radiating phase began abruptly and without any distinct foreshock activity in the hours before the earthquake down to a magnitude of completeness of M 0. Neither was there any evidence of tremor or other correlated seismic energy in the band between 0.1 and 5 Hz, or non-cultural signals in the 1-20 Hz band (White and Ellsworth, 1993). Two borehole strainmeters located 37 and 42 km southeast of the epicenter further constrain precursory deformation in the weeks to minutes before the earthquake. No strain changes exceeding 1 nanotesla were observed (Johnston et al., 1990).

The initiation of the earthquake was complex (Dietz and Ellsworth, 1997; Ellsworth, 2019). It began abruptly, with the first-arriving impulsive P wave strong enough to clip nearby short period seismometers within 0.02 s, but not strong enough to trigger many analog strong motion instruments. The initial rupture reached a plateau in seismic moment rate around 1 s into the (Beroza and Ellsworth, 1996). By 1.6 s into the event the seismic moment had grown to the equivalent of a M_W 5.6 earthquake. At this point, the moment rate jumped, marking the end of the seismic nucleation phase as defined by Beroza and Ellsworth (1996). These large, high-frequency waves arriving 1.6 s into the event have been interpreted as the beginning of the mainshock (Beroza, 1991). Relative to the initial hypocenter, this second nucleation locates 0.3 km southwest (along strike) and 1.1 km shallower (up dip) from the initial hypocenter(Dietz and Ellsworth, 1997). Modeling of the available strong motion accelerograms permit the interpretation of the initiator event as either a separate foreshock or the beginning of continuous moment release that slowed for a fraction of a second before propagating away from the initial hypocenter (Ellsworth, 2019).

Perhaps the main takeaway from Loma Prieta is that earthquakes should be expected to happen without warning on unknown faults even along the most closely monitored and studied fault systems.

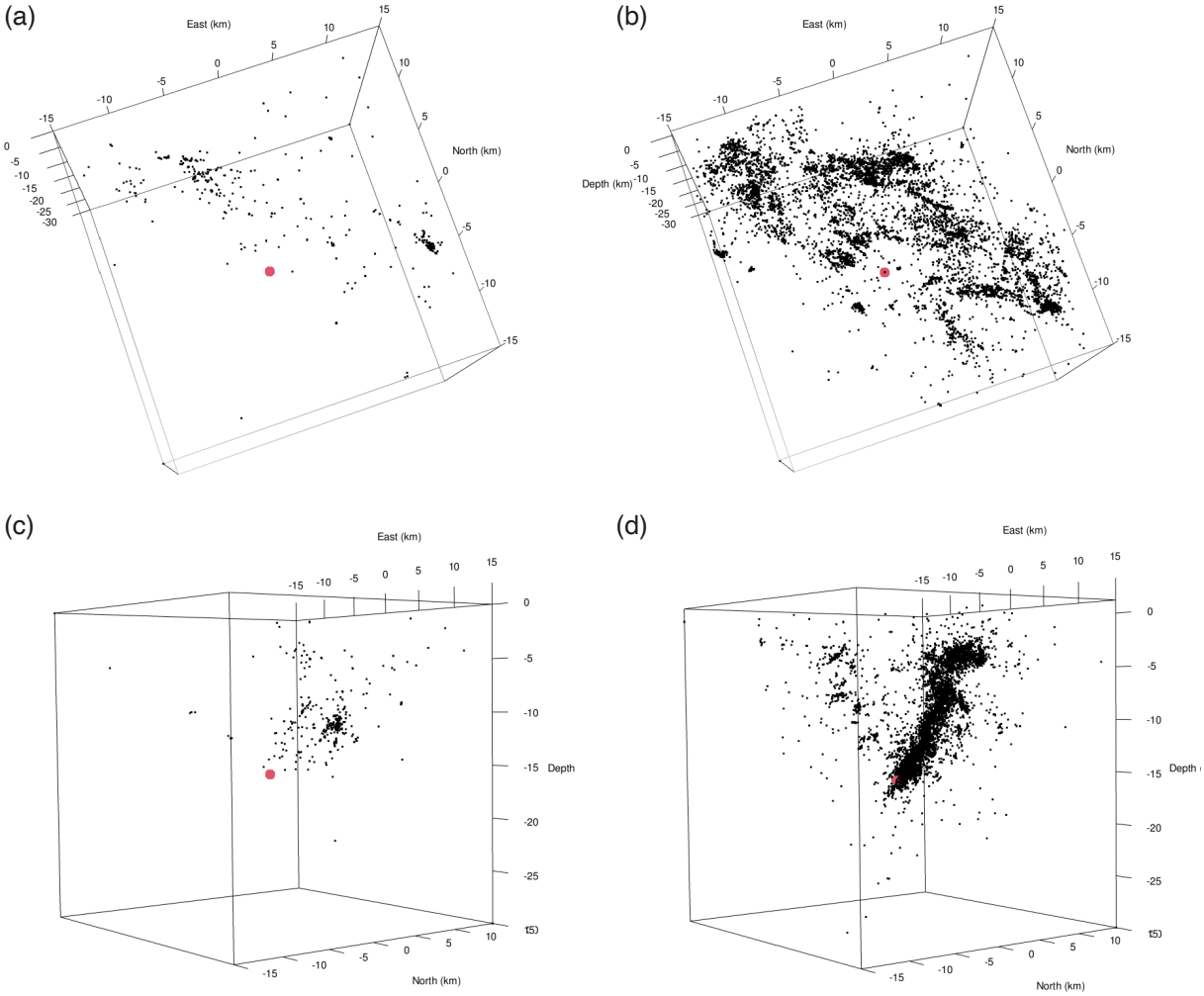

Figure 10. Multiple views of Double Difference seismicity associated with the 1989 M_W 7.0 Loma Prieta earthquake. Panels (a) and (c) show seismicity from 1984 to mainshock (red dot). Panels (b) and (d) show seismicity from mainshock through 2021.

6.4 M_W 6.5 San Simeon Earthquake of December 22, 2003

In almost a mirror image to the Coalinga earthquake 20 years earlier, the San Simeon earthquake ruptured reverse faults in the Oceano Fault System (Fig. 1). Faulting did not breach the surface. The earthquake and its aftershocks reveal a northeastward dipping main fault plane and steeply dipping back thrust (Hardebeck et al., 2004). Hauksson et al. (2004) obtained precision locations using a 3D velocity structure and hypoDD that place the aftershock volume with elevated Vp/Vs ratios, suggesting elevated pore pressures. The mainshock fault plane, however, was largely devoid of aftershocks, particularly near the hypocenter, suggesting an almost total stress drop.

With almost 2 decades of precision seismicity preceding the earthquake in the Double Difference catalog of Waldhauser and Schaff (2008), the event provides an excellent opportunity to examine the relationship between the prior activity and the earthquake. In map view (Fig. 11), the area within and around the earthquake was seismically active, but no more so than other areas. A perspective view of the prior activity and first 30 days of aftershocks indicates that some of the preceding activity localized on the mainshock and backthrust fault planes, or at least one with very similar location and dip (Fig. 12).

To look at the evolution of seismicity near the hypocenter, earthquake within a radial distance of 5 km from 1984 through the first month of aftershock activity are shown in Fig. 13. The magnitude of completeness for this volume is about M_D 1.5 with a b-value of 0.8. Only 3 earthquakes from the preceding 20 years located within 1 km of the hypocenter, the largest two in 1984, M_D 3.0 and 2.7, and the later one in 2001, M_D 1.9. Overall, the nearest large event, M_L 4.0 occurred in 1990 at almost 5 km distance. On a larger scale, one event, M_D 1.3 occurred 8 km from

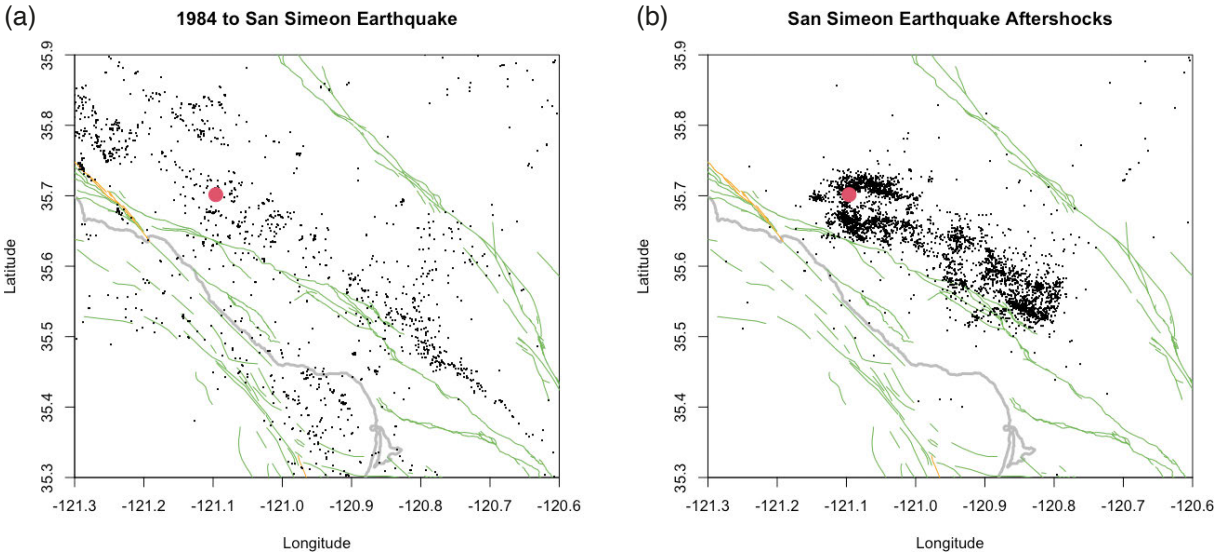

Figure 11. Seismicity in the region around the M_W 6.5 2003 San Simeon earthquake, preceding the earthquake from 1984 to mainshock (a), and in the first month of the aftershock sequence (b). Red dot marks the epicenter of the earthquake. Quaternary faults in green and Holocene faults in orange. Coastline in gray.

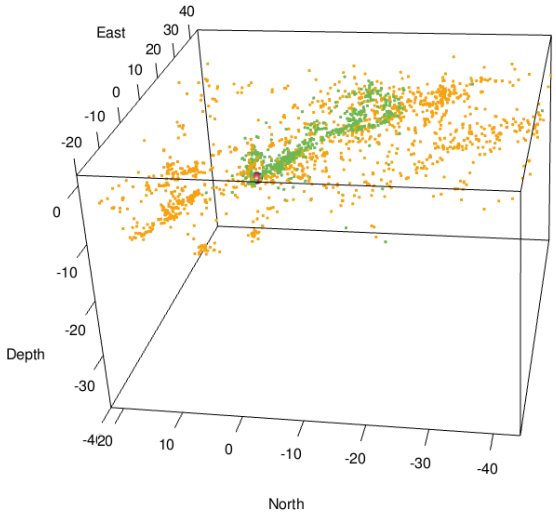

Figure 12. Perspective view looking northeast of seismicity preceding and following the M_W 6.5 2003 San Simeon earthquake. Hypocenter (red sphere with a radius of km). Preceding seismicity 1984 to mainshock in orange; one month of aftershocks MD ≥ 2.5 in green.

the hypocenter in the 24 hours before, and two M_D 1.5 and 1.9 17 km away three days before. It would be difficult to make the case that the seismicity rate changed in any significant way, either up or down, before the mainshock.

6.5 M_W 6.0 Parkfield Earthquake of September 28, 2004

The 40-km-long Parkfield segment of the San Andreas Fault is perhaps the most monitored, researched, discussed and debated fault anywhere. Systematic seismic monitoring began in 1967, shortly after the 1966 M_L 6.0 earthquake. In the mid-1980s the USGS and California Geological Survey joined forces to greatly expand the monitoring program with a wide variety of geophysical sensors designed to obtain a detailed understanding of seismicity, ground motion, strain, magnetic field, groundwater levels and fault creep with a commitment to issue a public alert of an impending earthquake if specific criteria were met (Bakun et al., 1987). When the earthquake happened, about

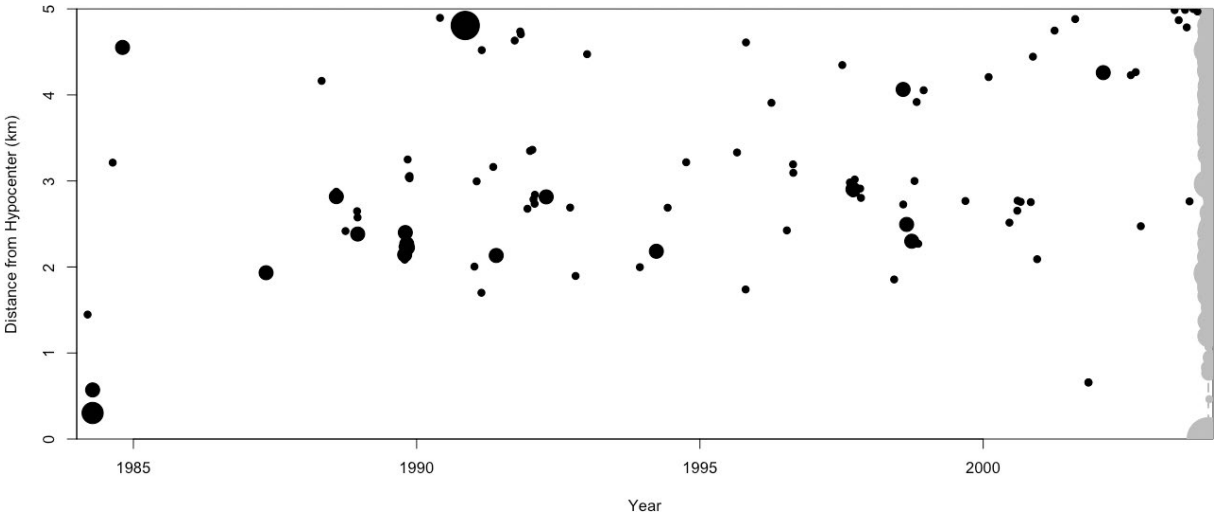

Figure 13. Space-time plot of seismicity near the hypocenter of the M_W 6.5 2003 San Simeon earthquake from 1984 to 1 month after the earthquake. Distance is radial to the hypocenter. Symbol size scales with magnitude. Preshocks in black and aftershocks in gray.

a decade later than anticipated, it occurred without any detectable precursory phenomena on any geophysical monitoring network, placing very strong constraints on hypothetical precursors such accelerating aseismic slip (Bakun et al., 1995; Johnston et al., 2006). Neither foreshocks ($M_D > 0$) nor slow strain transients ($M_W > 2$) occurred in the hours preceding the earthquake.

Our focus here is on the narrower question of seismicity evolution across the seismic cycle for earthquakes on San Andreas Fault (Fig. 14). Events within 750 m of the surface trace are defined here as on-fault activity. Like what was found for each of the other large earthquakes discussed above, there was no significant change in seismicity near the 2004 hypocenter as the time of the mainshock approached (Fig. 15). Activity at several km range remained elevated in the aftershock period through approximately 2012, if not beyond. Within 1 km of the hypocenter, four events occurred before in 1986, 1993, 1995 and 2000, M_D 3.0, 2.6, 1.5 and 1.2, respectively. A M_D 2.3 event also

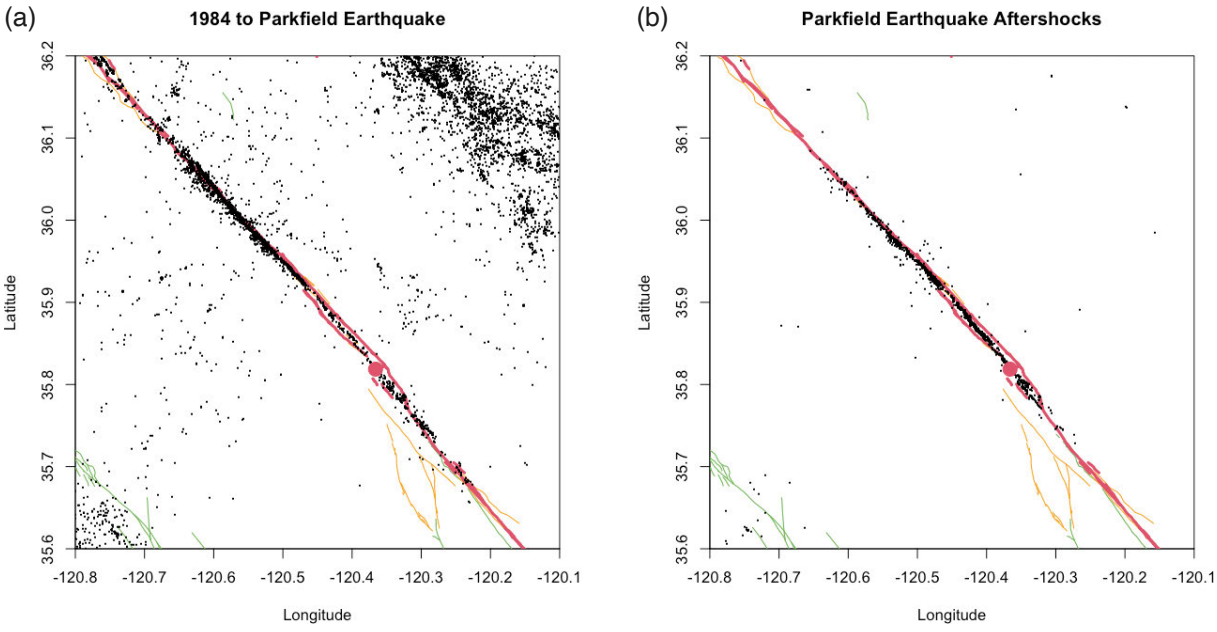

Figure 14. Seismicity in the region around the M_W 6.0 2004 Parkfield earthquake, preceding the earthquake from 1984 to mainshock (a), and in the first month of the aftershock sequence (b). Red dot marks the epicenter of the earthquake. Quaternary faults in green, Holocene faults in orange and historic ruptures in red.

followed the mainshock in 2008. The three earliest events are within a few hundred meters of the 2004 nucleation point, and quite possibly contain it within their rupture areas. However, these events are unremarkable in every other aspect.

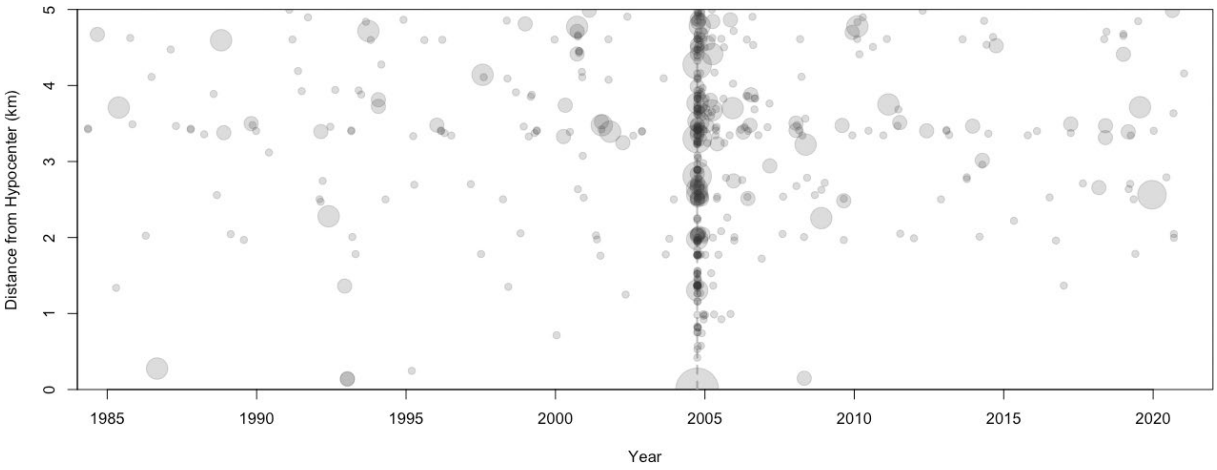

Figure 15. Space-time plot of seismicity near the hypocenter of the M_W 6.0 2004 Parkfield earthquake from 1984 through 2021. Distance is radial to the hypocenter. Symbols scale with magnitude.

Using the standard NCSN catalog covering 1969-1983 along with the double difference catalog from 1984 through 2021 and its extension with the real-time double difference catalog through August 2024 the spatial and temporal evolution of seismicity along the Parkfield segment can be examined in greater detail. The along-strike cross sections from these combined catalogs in Fig. 16 reveal remarkable organization of the seismicity throughout the seismic cycle. In particular, the streaks of repeating earthquake multiplets and the areas nearly devoid of seismicity they surround define stable features that are almost unaffected by the 2004 mainshock. It is notable that these features were described before the 2004 earthquake (Waldhauser et al., 2004) and correctly outlined the principal rupture area of the earthquake in the "hole" between 5 and 10 km depth between –20 and 10 km along strike. The repetition of the spatial pattern before and after the 2004 earthquake is also remarkable, and while it cannot be confirmed in the standard catalog locations from 1969-1983 it is strongly suggested (Fig. 16).

To further investigate the spatial-temporal evolution of seismicity, all dthe available catalog data, including the 1966 aftershocks (Eaton et al., 1970b) are combined to cover one complete seismic cycle and 20 years of the next (Fig. 17). Perhaps the most striking pattern is the spatial and temporal continuity of activity in the streaks where they appear as spatially narrow and temporally extended trains of events. There are also some notable temporal changes as well. Aftershocks of the 1966 earthquake extend about 5 kilometers further southeast than the 2004 earthquake. The opposite might be the case for 2004. However, the detection and location of aftershocks at the northwest end in 1966 was limited due to limitations of the aftershock station deployment (Eaton et al., 1970b). The aftershocks of 2004 blend into the background within 4 years of the mainshock. One exception lies beyond the southeastern end of both the 1966 and 2004 ruptures (10 to 20 km in Fig. 17) where the rate is slightly elevated. Likely unruptured since the great 1857 earthquake, only time will tell when it moves next.

Will there be another characteristic Parkfield earthquake, and when might it occur? The known catalog of the sequence, starting with the foreshocks to the 1957 earthquake is well-described by the Brownian Passage Time model with a mean of 25 years and aperiodicity of 0.44 (Ellsworth et al., 1999). According to this model the conditional probability at present is about 10%/year likelihood of the next event. Such a simple point process analysis fails to capture additional complexities of the Parkfield situation, particularly the building slip deficit on the Parkfield segment. Murray and Langbein (2006) document over 1 m of deficit on the 1966 and 2004 segments and over 2 m to the south since the 1934 earthquake. In addition, diminishing effects of the 1857 earthquake in models that include viscoelastic effects can lead to lengthening recurrence intervals (Ben Zion et al., 1993). Someday the fault will catch up with the plate motion and while we may not know when, Parkfield remains one of the best places to capture the pre- co- and post-seismic processes just as it was when selected for intensified monitoring 40 years ago.

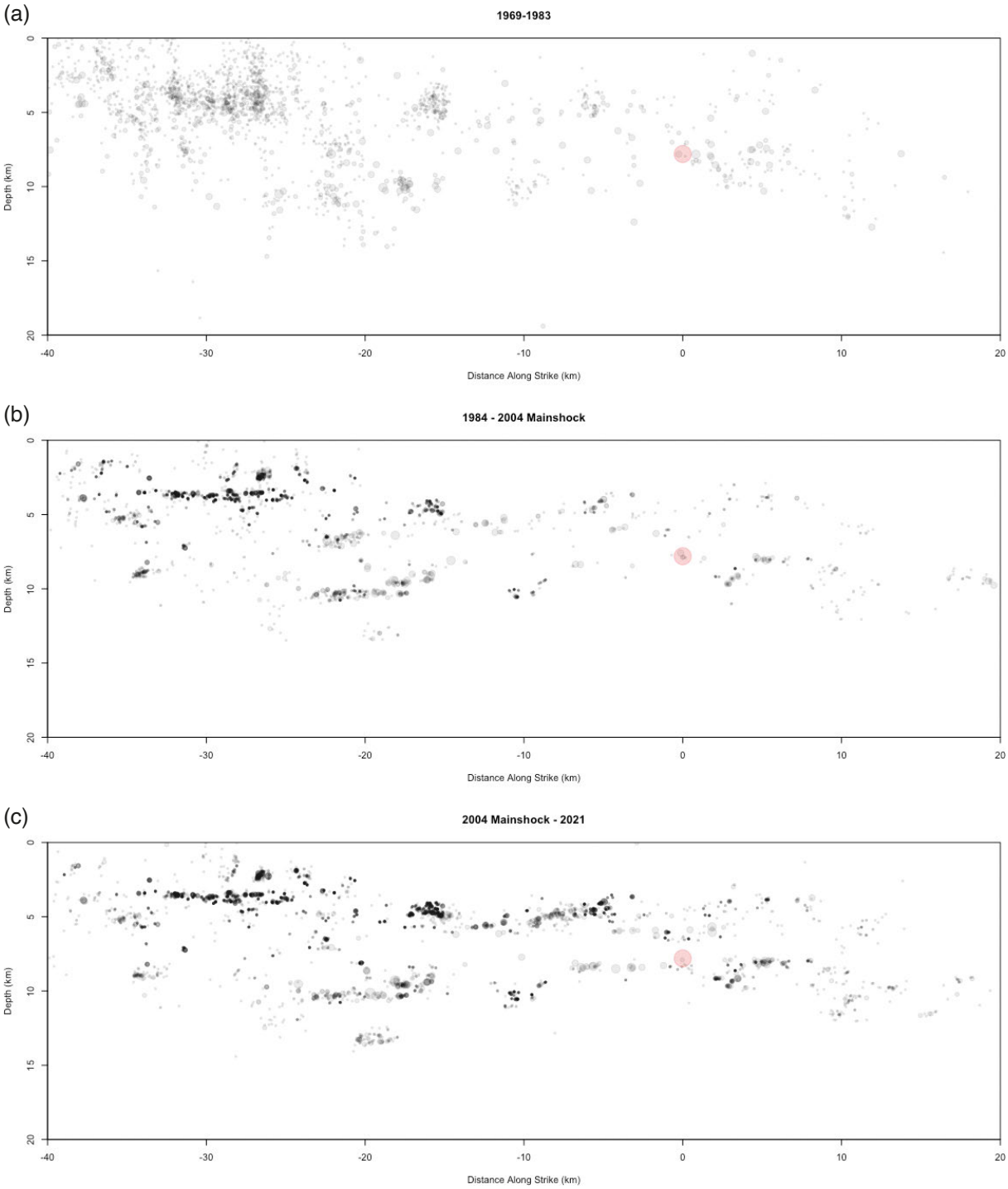

Figure 16. Fault parallel cross sections of seismicity on the San Andreas Fau lt in the vicinity of the M_W 6.0 2004 Parkfield earthquake. Mainshock hypocenter shown as translucent red circle. Symbols scale with magnitude. (a) NCSN catalog locations from 1969 through 1983. (b) Double Difference locations from 1984 to mainshock. (c) Double Difference locations from mainshock through 2021.

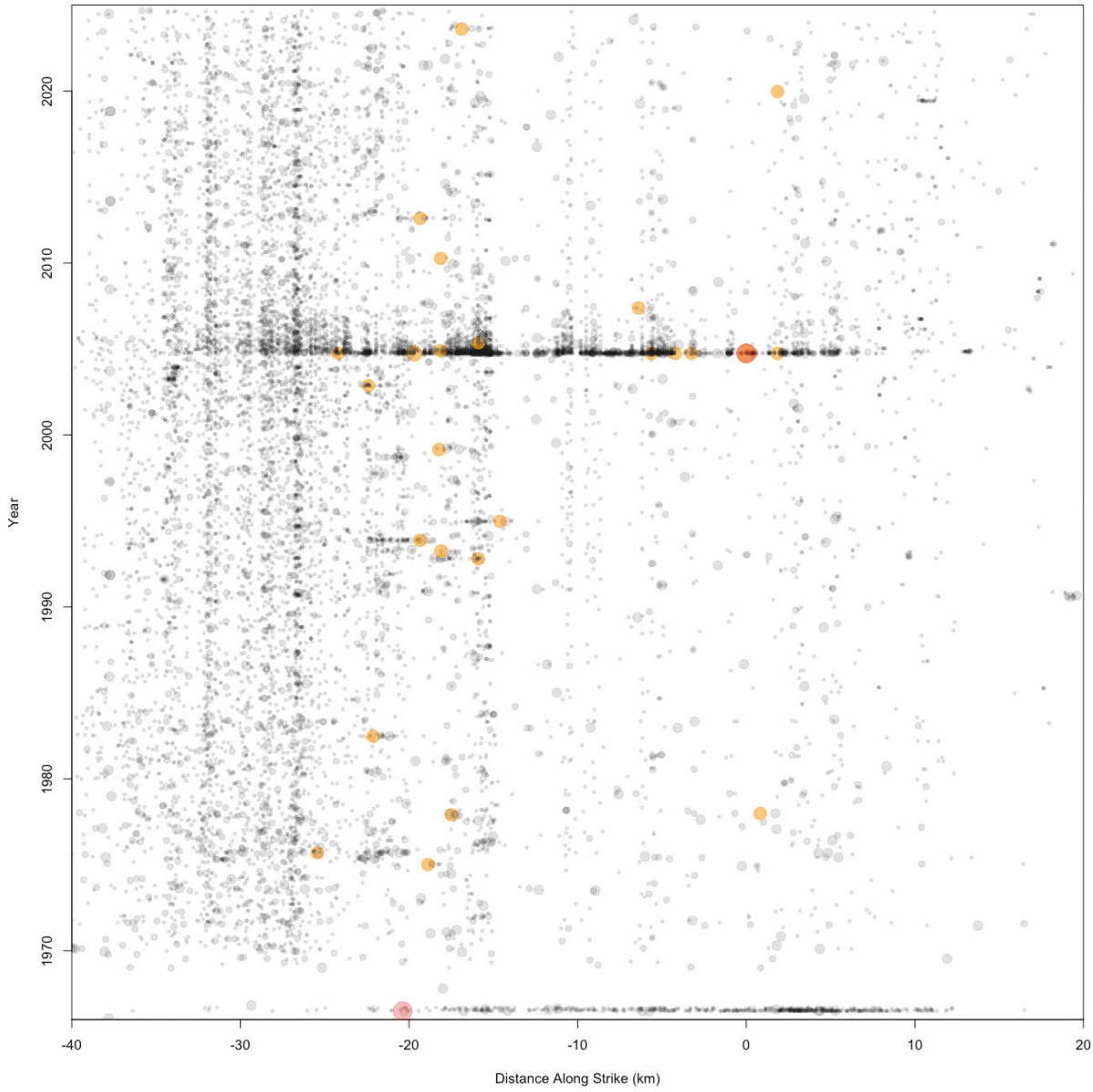

Figure 17. Space-time plot of Parkfield seismicity 1966-2024. Epicenters of the 1966 and 2004 mainshocks shown by translucent red circle. Earthquakes M ≥ 4 in orange, smaller events in gray. Symbols scale with magnitude. Aftershocks of the 1966 earthquake from Eaton et al. (1970b). NCSN catalog for 1969 through 1983. Double Difference locations for 1984 through 2021 and Real-Time Double Difference locations from 2022 through August 2024. Note data gap following 1966 earthquake to start of NCSN catalog in 1969.

6.6 M_W 6.0 South Napa Earthquake of August 24, 2014

If the other M 6+ events discussed above were or could have been anticipated at least to some degree based on prior seismicity, the South Napa earthquake was a surprise (Fig. 18). It ruptured the surface along 12 km of the pre-Holocene West Napa fault to the north of the epicenter (Brocher et al., 2015). At depth, the rupture propagated 15 km unilaterally north from the epicenter (Wei et al., 2015), with aftershocks spreading both south and north an additional 5-10 km over the next month. In the immediate epicentral area little seismicity was detected in the preceding 43 years despite being in the core monitoring area of the NCSN since the early 1970s (Fig. 18). The only 5 events locate within 3 km of the hypocenter, none as large as M_D 2.0 and none after 2009.

The only clear seismicity evidence for the fault lies north rupture, where it defines a liner, near vertical fault that meets the northern end of the aftershock zone. It serves as a reminder that small faults resolved by precision seismicity can hint at a hazard poised by larger structures even where careful geologic mapping identifies no active faults.

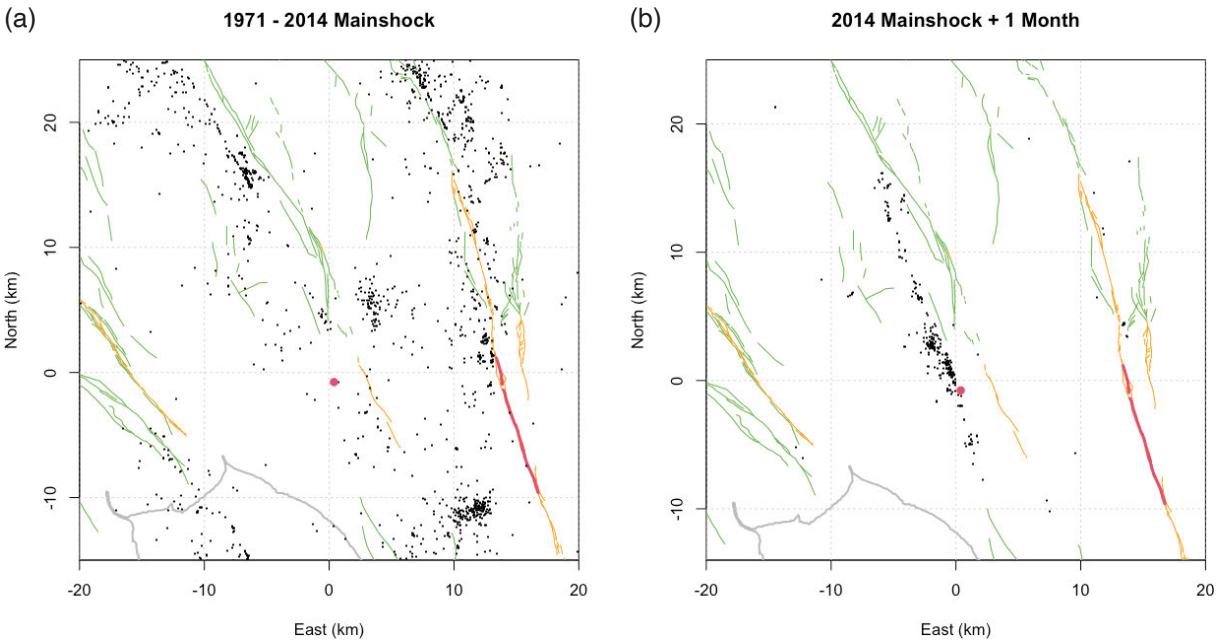

Figure 18. Seismicity in the region around the M_W 6.0 2014 South Napa earthquake, preceding the earthquake from 1971 to mainshock (a), and in the first month of the aftershock sequence (b). Red dot marks the epicenter of the earthquake. Quaternary faults in green, Holocene faults in orange and historic ruptures in red. Shoreline of San Pablo Bay in gray.

7. Discussion

The patterns of seismicity preceding and following the six M 6+ earthquakes discussed above share several common features as well as having significant differences. None of them display a build-up of seismicity in the months, weeks, days, hours or minutes before the mainshock. Only the 1984 Morgan Hill event had foreshocks within 6 orders of magnitude of the mainshock (7 orders of magnitude for Loma Prieta), and then only two undistinguished events of $M_D < 1$. If earthquakes are preceded by accelerating slip in a nucleation zone larger than laboratory dimensions (McLaskey, 2019) one may ask why did it fail to manifest itself in seismicity for any these events? Perhaps the answer is that in nature the nucleation process occurs over scale lengths little different from those measured in the laboratory, which are far too small to be detected at the surface (Ellsworth, 2019).

Over longer time scales, very light seismicity occurred in the preceding decades within several km of the mainshock hypocenter for all these events. The 1934 and 1966 Parkfield earthquakes are central California counterexamples (Bakun and McEvilly, 1984), although it should be noted that the public alerts triggered by events in the 1934/1966 hypocentral zone in 1992 and 1993 (Fig. 17) failed to initiate the earthquake.

Precision seismicity on a larger scale revealed, or at least hinted at the fault before the mainshock in five of the six cases. The faults were most clearly defined for the strike slip Morgan Hill and Parkfield events, which perhaps is no surprise as both exhibit abundant repeating earthquakes that continued through the mainshock without significant spatial evolution. The faults that ruptured in the reverse faulting Coalinga and San Simeon earthquake are not as well defined, partly due to their location on the edges of the seismic network. The clear exception, Loma Prieta was also the societally most consequential. It serves as a caution that unexpected earthquakes will occur in the future on faults that give little or no indication of their presence or proximity to failure.

8. Outlook

Rapid advances in the application of deep learning methods to earthquake seismology, including the detection, identification and timing of seismic phase are continuing to revolutionize the analysis and interpretation of seismicity on local and regional scales globally (Mousavi and Beroza, 2022). The outcrop scale resolution of seismic structures

achievable with the methods of precision seismicity have transformed our understanding of crustal seismicity in all tectonic settings and on multiple scales. Studies of normal faults in Italy, for example reveal the complex segmentation of faulting (Chiaraluce et al., 2003), enigmatic very low angle normal faults (Chiaraluce, 2007) and through complex, extended sequences (Tan et al., 2021; Chiaraluce et al., 2022). Low magnitude fluid driven seismicity in California found in both volcanic (Shelly et al., 2016) and tectonic (Ross et al., 2019) settings demonstrates the power of precision seismicity methods to detect anomalous activity against the drumbeat of the tectonic background. Perhaps nowhere have the tools had a greater impact than on the analysis and understanding of induced seismicity, establishing causal relations between industrial drivers and consequential earthquakes (Woo et al., 2019) and revealing the previously unknown architecture of the basement in response to pore pressure forcing (Park et al., 2020 and 2022).

The study of seismicity, as advanced by precision seismicity is far from done or fully developed. There is a great need for new methods to routinely determine precision focal mechanisms and earthquake source parameters including rupture area and directivity. The study of repeating earthquakes and temporal variations in crustal properties that they can reveal, as first demonstrated decades ago (Poupinet et al., 1984) represents another powerful but underutilized pathway for deepening our understanding of faults and active tectonic processes.

Data availability statement. Data can be downloaded at: https://ncedc.org/.

Acknowledgements. Over the course of my career, I have had the privilege to learn from and work with a host of seismologists, many of whom share my interest in the hypocenter problem. It would be impossible to list them all, but I would like to acknowledge the ideas, insights and contributions to the development of precision seismicity from Rob Wesson, Willie Lee, David Hill, Steve Roecker, Cliff Thurber, Georges Poupinet, Julien Frechet, Edi Kissling, Greg Beroza, Nicholas Deichmann, Stephanie Prejean, Felix Waldhauser, David Schaff, Lauro Chiaraluce, Kaz Imanishi, David Shelly, Jeong-Ung Woo and Yongsoo Park. This work would not have been possible without the commitment of the Earthquake Hazards Reduction Program of the U.S. Geological Survey to engage in strategic research or the skill and dedication of the NCSN staff who built, operated and analyzed the network. I am also deeply indebted to David Oppenheimer, Felix Waldhauser and David Schaff for their catalogs of northern California seismicity used in this study. I also thank Maria Teresa Mariucci and Paola Montone for their helpful reviews of the manuscript. The Northern California Earthquake Data Center is gratefully acknowledged as the home for the catalogs used in this study, along with the waveform repository on which precision seismicity is based.

References

Bakun, W. H., M. M. Clark, R. S. Cockerham, W. L. Ellsworth et al. (1984). The 1984 Morgan Hill, California, earthquake, Science, 225, 4659, 288-291, doi:10.1126/science.225.4659.288.

Bakun, W. H. and T. V. McEvilly (1984). Recurrence models and Parkfield, California, earthquakes, J. Geophys. Res., Solid Earth, 89, B5, 3051-3058, doi:10.1029/JB089iB05p03051.

Bakun, W. H., K. S. Breckenridge, J. D. Bredehoeft, R. O. Burford et al. (1987). Parkfield, California, earthquake prediction scenarios and response plans, U. S. Geol. Surv. Open-File Rep., 87-192, doi:10.3133/ofr87192.

Bakun, W. H., B. Aagaard, B. Dost, W. L. Ellsworth et al. (2005). Implications for prediction and hazard assessment from the 2004 Parkfield earthquake, Nature, 437, 7061, 969-974, doi:10.1038/nature04067.

Ben-Zion, Y., J. R. Rice and R. Dmowska (1993). Interaction of the San Andreas fault creeping segment with adjacent great rupture zones and earthquake recurrence at Parkfield, J. Geophys. Res., Solid Earth, 98, B2, 2135-2144, doi:10.1029/92JB02154.

Beroza, G. C. (1991). Near-source modeling of the Loma Prieta earthquake: Evidence for heterogeneous slip and implications for earthquake hazard, B. Seismol. Soc. Am., 81, 5, 1603-1621, doi:10.1785/BSSA0810051603.

Beroza, G. C. and M. D. Zoback (1993). Mechanism diversity of the Loma Prieta aftershocks and the mechanics of mainshock-aftershock interaction, Science, 259, 5092, 210-213, doi:10.1126/science.259.5092.210.

Beroza, G. C. and W. L. Ellsworth (1996). Properties of the seismic nucleation phase, Tectonophysics, 261, 1-3, 209-227, doi:10.1016/0040-1951(96)00067-4.

Brocher, T. M., A. S. Baltay, J. L. Hardebeck, F. F. Pollitz et al. (2015). The M w 6.0 24 august 2014 south napa earthquake, Seismol. Res. Lett., 86, 2A, 309-326, doi:10.1785/0220150004.

Chiaraluce, L., W. L. Ellsworth, C. Chiarabba and M. Cocco (2003). Imaging the complexity of an active normal fault system: The 1997 Colfiorito (central Italy) case study, J. Geophys. Res., Solid Earth, 108, B6, doi:10.1029/2002JB002166.

Chiaraluce, L., C. Chiarabba, C. Collettini, D. Piccinini et al. (2007). Architecture and mechanics of an active low-angle normal fault: Alto Tiberina fault, northern Apennines, Italy, J. Geophys. Res., Solid Earth, 112, B10, doi:10.1029/2007JB005015.

Chiaraluce, L., M. Michele, F. Waldhauser, Y. J. Tan et al. (2022). A comprehensive suite of earthquake catalogues for the 2016-2017 Central Italy seismic sequence, Sci. Data, 9, 1, 710, doi:10.1038/s41597-022-01827-z.

Crosson, R. S. (1976). Crustal structure modeling of earthquake data: 1. Simultaneous least squares estimation of hypocenter and velocity parameters, J. Geophys. Res., 81, 17, 3036-3046, doi:10.1029/JB081i017p03036.

Deichmann, N. and M. Garcia-Fernandez (1992). Rupture geometry from high-precision relative hypocentre locations of microearthquake clusters, Geophys. J. Int., 110, 3, 501-517, doi:10.1111/j.1365-246X.1992.tb02088.x.

Dietz, L. D. and W. L. Ellsworth (1990). The October 17, 1989, Loma Prieta, California, earthquake and its aftershocks: Geometry of the sequence from high-resolution locations, Geophys. Res. Lett., 17, 9, 1417-1420, doi:10.1029/GL017i009p01417.

Dietz, L. D. and W. L. Ellsworth (1997). Aftershocks of the Loma Prieta earthquake and their tectonic implications, U. S. Geol. Surv. Prof. Pap., 1550D, D5-D47.

Dodge, D. A., G. C. Beroza and W. L. Ellsworth (1995). Foreshock sequence of the 1992 Landers, California, earthquake and its implications for earthquake nucleation, J. Geophys. Res., Solid Earth, 100, B6, 9865-9880, doi:10.1029/95JB00871.

Dodge, D. A., G. C. Beroza and W. L. Ellsworth (1996). Detailed observations of California foreshock sequences: Implications for the earthquake initiation process, J. Geophys. Res., Solid Earth, 101, B10, 22371-22392, doi:10.1029/96JB02269.

Eberhart-Phillips, D. and P. A. Reasenberg (1990). Complex faulting structure inferred from local seismic observations of M ≥ 1.0 aftershocks, May 2-June 30, 1983, in The Coalinga, California, Earthquake of May 2, 1983, M. J. Rymer and W. L. Ellsworth (Eds.), U. S. Geol. Surv. Prof. Pap. 1487, Washington, 171-192.

Eaton, J. P. (1966). HYPOLAYR, a computer program for determining hypocenters of local earthquakes in an earth consisting of uniform flat layers over a half space, U. S. Geol. Surv. Open-File Rep., doi:10.3133/ofr6985.

Eaton, J. P., W. H. K. Lee and L. C. Pakiser (1970a). Use of microearthquakes in the study of the mechanics of earthquake generation along the San Andreas fault in central California, Tectonophysics, 9, 2-3, 259-282, doi:10.1016/0040-1951(70)90021-1.

Eaton, J. P., M. E. O'Neill and J. N. Murdock (1970b). Aftershocks of the 1966 Parkfield-Cholame, California, earthquake: A detailed study, Bull. Seismol. Soc. Am., 60, 4, 1151-1197.

Eaton, J. P. (1990). The earthquake and its aftershocks from May 2 through September 30, 1983, in The Coalinga, California, Earthquake of May 2, 1983, M. J. Rymer and W. L. Ellsworth (Eds.), U. S. Geol. Surv. Prof. Pap. 1487, Washington, 113-170.

Ellsworth, W. L. (1975). Bear valley, California, earthquake sequence of February-March 1972, Bull. Seismol. Soc. Am., 65, 2, 483-506, doi:10.1785/BSSA0650020483.

Ellsworth, W. L. (1995). Characteristic earthquakes and long-term earthquake forecasts: Implications of central California seismicity. In Urban disaster mitigation: The role of engineering and technology, Pergamon (Ed.), 1-14, doi:10.1016/B978-008041920-6/50007-5.

Ellsworth, W. L., M. V. Matthews, R. M. Nadeau, S. P. Nishenko et al. (1999). A physically-based earthquake recurrence model for estimation of long-term earthquake probabilities, U. S. Geol. Surv. Open-File Rep., 99-522, doi:10.3133/ofr99522.

Ellsworth, W. L. (2019). From foreshocks to mainshocks: mechanisms and implications for earthquake nucleation and rupture propagation. In Mechanics of Earthquake Faulting, IOS Press, 95-112, doi:10.3254/978-1-61499-979-9-95.

Field, E. H., R. J. Arrowsmith, G. P. Biasi, P. Bird et al. (2014). Uniform California earthquake rupture forecast, version 3 (UCERF3) – The time-independent model, Bull. Seismol. Soc. Am., 104, 3, 1122-1180, doi:10.1785/0120130164.

Got, J. L., J. Fréchet and F. W. Klein (1994). Deep fault plane geometry inferred from multiplet relative relocation beneath the south flank of Kilauea, J. Geophys. Res., Solid Earth, 99, B8,15375-15386, doi:10.1029/94JB00577.

Hardebeck, J. L., J. Boatwright, D. Dreger, R. Goel et al. (2004). Preliminary report on the 22 December 2003, m 6.5 San Simeon, California earthquake, Seismol. Res. Lett., 75, 2, 155-172, doi:10.1785/gssrl.75.2.155.

Harris, R. A. (1998). Forecasts of the 1989 Loma Prieta, California, earthquake, Bull. Seismol. Soc. Am., 88, 4, 898-916, doi:10.1785/BSSA0880040898.

Harris, R. A. (1998). The Loma Prieta, California, Earthquake of October 17, 1989 Forecasts, U. S. Geol. Surv. Prof. Pap., 1550-B, doi:10.3133/pp1550.

Hauksson, E., D. Oppenheimer and T. M. Brocher (2004). Imaging the source region of the 2003 San Simeon earthquake within the weak Franciscan subduction complex, central California, Geophys. Res. Lett., 31, 20, doi:10.1029/2004GL021049.

Hileman, J. A., C. R. Allen and J. M. Nordquist (1973). Seismicity of the Southern California Region 1 January 1932 to 31 December 1972, Seismological Laboratory California Institute of Technology.

Hill, D. P., J. P. Eaton and L. M. Jones (1990). Seismicity, 1980-86, Geol. Surv. Prof. Pap., USA, 1515.

Johnston, M. J. S., A. T. Linde and M. T. Gladwin (1990). Near-field high resolution strain measurements prior to the October 18, 1989, Loma Prieta Ms 7.1 Earthquake, Geophys. Res. Lett., 17, 10, 1777-1780, doi:10.1029/GL017i010p01777.

Johnston, M. J. S., J. A. Olson, A. C. Fraser-Smith, A. Bernardi et al. (1993). The Loma Prieta, California, Earthquake of October 17, 1989, Preseismic Observations, U. S. Geol. Surv. Prof. Pap., 1550-C, doi:10.3133/pp1550C.

Johnston, M. J. S., R. D. Borcherdt, A. T. Linde and M. T. Gladwin (2006). Continuous borehole strain and pore pressure in the near field of the 28 September 2004 M 6.0 Parkfield, California, earthquake: Implications for nucleation, fault response, earthquake prediction and tremor, Bull. Seismol. Soc. Am., 96, 4B, S56-S72, doi:10.1785/0120050822.

Kissling, E., W. L. Ellsworth, D. Eberhart-Phillips and U. Kradolfer (1994). Initial reference models in local earthquake tomography, J. Geophys. Res., Solid Earth, 99, B10, 19635-19646, doi:10.1029/93JB03138.

Kissling, E., U. Kradolfer and H. Maurer (1995). Program VELEST user's guide-Short Introduction, Institute of Geophysics, ETH Zurich.

Klein, F. W. (2002). User's guide to HYPOINVERSE-2000, a Fortran program to solve for earthquake locations and magnitudes, U. S. Geol. Surv. Open-File Rep., 2002-171, doi:10.3133/ofr02171.

Lahr, J. C. (1989). HYPOELLIPSE/version 2.0; a computer program for determining local earthquake hydrocentral parameters, magnitude, and first motion pattern, U. S. Geol. Surv. Open-File Rep., 89-116, doi:10.3133/ofr89116.

Lee, W. H. and J. C. Lahr (1975). HYPO71 revised; a computer program for determining hypocenter, magnitude, and first motion pattern of local earthquakes, U. S. Geol. Surv. Open-File Rep., 75-311, doi:10.3133/ofr75311.

Lin, G. and P. Shearer (2006). The COMPLOC earthquake location package, Seismol. Res. Lett., 77, 4, 440-444, doi:10.1785/gssrl.77.4.440.

Lindh, A. (1983). Preliminary assessment of long-term probabilities for large earthquakes along selected fault segments of the San Andreas fault system, California, U. S. Geol. Surv. Open-File Rep., 83-63, 14, doi:10.3133/ofr8363.

Lomax, A. and A. Savvaidis (2022). High-precision earthquake location using source-specific station terms and inter-event waveform similarity, J. Geophys. Res., Solid Earth, 127, 1, p.e2021JB023190, doi:10.1029/2021JB023190.

Marone, C., J. E. Vidale and W. L. Ellsworth (1995). Fault healing inferred from time dependent variations in source properties of repeating earthquakes, Geophys. Res. Lett., 22, 22, 3095-3098, doi:10.1029/95GL03076.

McGarr, A. (1991). On a possible connection between three major earthquakes in California and oil production, Bull. Seismol. Soc. Am., 81, 3, 948-970, doi:10.1785/BSSA0810030948.

McLaskey, G. C. (2019). Earthquake initiation from laboratory observations and implications for foreshocks, J. Geophys. Res., Solid Earth, 124, 12, 12882-12904, doi:10.1029/2019JB018363.

Michael, A. J., W. L. Ellsworth and D. H. Oppenheimer (1990). Coseismic stress changes induced by the 1989 Loma Prieta, California earthquake, Geophys. Res. Lett., 17, 9, 1441-1444, doi:10.1029/GL017i009p01441.

Mousavi, S. M. and G. C. Beroza (2022). Deep-learning seismology, Science, 377, 6607, p.eabm4470, doi:10.1126/science.abm4470.

Murray, J. and J. Langbein (2006). Slip on the San Andreas Fault at Parkfield, California, over two earthquake cycles, and the implications for seismic hazard, Bull. Seismol. Soc. Am., 96, 4B, S283-S303, doi:10.1785/0120050820.

Nadeau, R. M. and T. V. McEvilly (2004). Periodic pulsing of characteristic microearthquakes on the San Andreas fault, Science, 303, 5655, 220-222, doi:10.1126/science.1090353.

Nakamura, Y. (1978). A1 moonquakes-source distribution and mechanism, in Lunar and Planetary Science Conference, 9th, Houston, Tex., March 13-17, 1978, Proceedings, Volume 3, A79-39253 16-91, Pergamon Press, Inc., New York, 3589-3607.

Park, Y., S. M. Mousavi, W. Zhu, W. L. Ellsworth et al. (2020). Machine-learning-based analysis of the Guy-Greenbrier, Arkansas earthquakes: A tale of two sequences, Geophys. Res. Lett., 47, 6, p.e2020GL087032, doi:10.1029/2020GL087032.

Park, Y., G. C. Berozaand and W. L. Ellsworth (2022). Basement fault activation before larger earthquakes in Oklahoma and Kansas, The Seismic Record, 2, 3, 197-206, doi:10.1785/0320220020.

Poupinet, G., W. L. Ellsworth and J. Frechet (1984). Monitoring velocity variations in the crust using earthquake doublets: An application to the Calaveras Fault, California, J. Geophys. Res., Solid Earth, 89, B7, 5719-5731, doi:10.1029/JB089iB07p05719.

Pujol, J. (1988). Comments on the joint determination of hypocenters and station corrections, Bull. Seismol. Soc. Am., 78, 3, 1179-1189, doi:10.1785/BSSA0780031179.

Reasenberg, P. A. (1997). The Loma Prieta, California, Earthquake of October 17, 1989: Aftershocks and Postseismic Effects, U. S. Geol. Surv. Prof. Pap., 1550-C., doi:10.3133/pp1550D.

Reasenberg, P. A. and W. L. Ellsworth (1982). Aftershocks of the Coyote Lake, California, earthquake of August 6, 1979: A detailed study, J. Geophys. Res., Solid Earth, 87, B13, 10637-10655.

Reasenberg, P. A. and R. W. Simpson (1997). Response of regional seismicity to the static stress change produced by the loma prieta earthquake, U. S. Geol. Surv. Prof. Pap., 1550-D, D49-D71, doi:10.1126/science.255.5052.1687.

Richards-Dinger, K. B. and P. M. Shearer (2000). Earthquake locations in southern California obtained using source-specific station terms, J. Geophys. Res., Solid Earth, 105, B5,10939-10960, doi:10.1029/2000JB900014.

Roecker, S. W. (1982). Velocity structure of the Pamir-Hindu Kush region: Possible evidence of subducted crust, J. Geophys. Res., Solid Earth, 87, B2, 945-959, doi:10.1029/JB087iB02p00945.

Ross, Z. E., D. T. Trugman, E. Hauksson and P. M. Shearer (2019). Searching for hidden earthquakes in Southern California, Science, 364, 6442, 767-771, doi:10.1126/science.aaw6888.

Rubin, A. M., D. Gillard and J. L. Got (1999). Streaks of microearthquakes along creeping faults, Nature, 400, 6745, 635-641, doi:10.1038/23196.

Rubinstein, J. L., W. L. Ellsworth, K. H. Chen and N. Uchida (2012). Fixed recurrence and slip models better predict earthquake behavior than the time and slip predictable models: 1. Repeating earthquakes, J. Geophys. Res., Solid Earth, 117, B2, doi:10.1029/2011JB008723.

Rubinstein, J. L. and G. C. Beroza (2004). Evidence for widespread nonlinear strong ground motion in the M_W 6.9 Loma Prieta earthquake, Bull. Seismol. Soc. Am., 94, 5, 1595-1608, doi:10.1785/012004009.

Rymer, M. J. and W. L. Ellsworth (1990). The Coalinga, California, Earthquake of May 2, 1983, U. S. Geol. Surv. Prof. Pap., 1487, 417, doi:10.3133/pp1487.

Schaff, D. P. and G. C. Beroza (2004). Coseismic and postseismic velocity changes measured by repeating earthquakes, J. Geophys. Res., Solid Earth, 109, B10, doi:10.1029/2004JB003011.

Schaff, D. P., G. H. Bokelmann, G. C. Beroza, F. Waldhauser et al. (2002). High-resolution image of Calaveras fault seismicity, J. Geophys. Res., Solid Earth, 107, B9, ESE-5, doi:10.1029/2001JB000633.

Segall, P. and R. F. Yerkes (1990). Stress and fluid-pressure changes associated with oil-field operations: A critical assessment of effects in the focal region of the earthquake, U. S. Geol. Surv. Prof. Pap., 1487, Chapter 14, 259-272.

Shelly, D. R., W. L. Ellsworth and D. P. Hill (2016). Fluid-faulting evolution in high definition: Connecting fault structure and frequency magnitude variations during the 2014 Long Valley Caldera, California, earthquake swarm, J. Geophys. Res., Solid Earth, 121, 3, 1776-1795, doi:10.1002/2015JB012719.

Sheng, Y., W. L. Ellsworth, A. Lellouch and G. C. Beroza (2021). Depth constraints on coseismic velocity changes from frequency dependent measurements of repeating earthquake waveforms, J. Geophys. Res., Solid Earth, 126, 2, p.e2020JB020421, doi:10.1029/2020JB020421.

Simpson, R. W. (1994). The Loma Prieta, California, Earthquake of October 17, 1989: Tectonic Processes and Models, U.S. Geol. Surv. Prof. Pap., 1550-F, doi:10.3133/pp1550F.

Smith, J. D., Z. E. Ross, K. Azizzadenesheli and J. B. Muir (2022). HypoSVI: Hypocentre inversion with Stein variational inference and physics informed neural networks, Geophys. J. Int., 228, 1, 698-710, doi:10.1093/gji/ggab309.

Spudich, P. (1997). The Loma Prieta, California, Earthquake of October 17, 1989: Main shock Characteristics, U. S. Geol. Surv. Prof. Pap., 1550-A, doi:10.3133/pp1550A.

Stein, R. S. and G. Ekström (1992). Seismicity and geometry of a 110 km long blind thrust fault 2. Synthesis of the 1982-1985 California earthquake sequence, J. Geophys. Res., Solid Earth, 97, B4, 4865-4883, doi:10.1029/91JB02847.

Tan, Y. J., F. Waldhauser, W. L. Ellsworth and M. Zhang (2021). Machine learning-based high-resolution earthquake catalog reveals how complex fault structures were activated during the 2016-2017 central Italy sequence, The Seismic Record, 1, 1, 11-19, doi:10.1785/0320210001.

Templeton, D., R. M. Nadeau and R. Bürgmann (2008). Behavior of repeating earthquake sequences in central California and the implications for subsurface fault creep, Bull. Seismol. Soc. Am., 98, 1, 52-65, doi:10.1785/0120070026.

Thurber, C. H. (1983). Earthquake locations and three-dimensional crustal structure in the Coyote Lake area, central California, J. Geophys. Res., Solid Earth, 88, B10, 8226-8236, doi:10.1029/JB088iB10p08226.

Trugman, D. T. and P. M. Shearer (2017). GrowClust: A hierarchical clustering algorithm for relative earthquake relocation, with application to the Spanish Springs and Sheldon, Nevada, earthquake sequences, Seismol. Res. Lett., 88, 2A, 379-391, doi:10.1785/0220160188.

Uchida, N. and R. Bürgmann (2019). Repeating earthquakes, Ann. Rev. Earth Planet Sci., 47, 1, 305-332, doi:10.1146/annurev-earth-053018-060119.

Vidale, J. E., W. L. ElIsworth, A. Cole and C. Marone (1994). Variations in rupture process with recurrence interval in a repeated small earthquake, Nature, 368, 6472, 624-626, doi:10.1038/368624a0.

Waldhauser, F. (2009). Near-real-time double-difference event location using long-term seismic archives, with application to Northern California, Bull. Seismol. Soc. Am., 99, 5, 2736-2748, doi:10.1785/0120080294.

Waldhauser, F., W. L. Ellsworth and A. Cole (1999). Slip-parallel seismic lineations on the northern Hayward fault, California, Geophys. Res. Lett., 26, 23, 3525-3528, doi:10.1029/1999GL010462.

Waldhauser, F. and W. L. Ellsworth (2000). A double-difference earthquake location algorithm: Method and application to the northern Hayward fault, California, Bull. Seismol. Soc. Am., 90, 6, 1353-1368, doi:10.1785/0120000006.

Waldhauser, F., W. L. Ellsworth, D. P. Schaff and A. Cole (2004). Streaks, multiplets, and holes: High-resolution spatio-temporal behavior of Parkfield seismicity, Geophys. Res. Lett., 31, 18, doi:10.1029/2004GL020649.

Waldhauser, F. and D. P. Schaff (2008). Large-scale relocation of two decades of Northern California seismicity using cross-correlation and double-difference methods, J. Geophys. Res., Solid Earth, 113, B8, doi:10.1029/2007JB005479.

Waldhauser, F. and D. P. Schaff (2021). A comprehensive search for repeating earthquakes in northern California: Implications for fault creep, slip rates, slip partitioning, and transient stress, J. Geophys. Res., Solid Earth, 126, 11, 2021JB022495, doi:10.1029/2021JB022495.

Wallace, R. E. (Ed.) (1990). The San Andreas Fault System, California, U. S. Geol. Surv. Prof. Pap., 1515, 293, doi:10.3133/pp1515.

Wei, S., S. Barbot, R. Graves, J. J. Lienkaemper et al. (2015). The 2014 M_W 6.1 South Napa earthquake: A unilateral rupture with shallow asperity and rapid afterslip, Seismol. Res. Lett., 86, 2A, 344-354, doi:10.1785/0220140249.

Wells, R. E. (2004). The Loma Prieta, California, Earthquake of October 17, 1989 – Geologic Setting and Crustal Structure, U. S. Geol. Surv. Prof. Pap., 1550-E, doi:10.3133/pp1550E.

Wesson, R. L. (1971). Travel-time inversion for laterally inhomogeneous crustal velocity models, Bull. Seismol. Soc. Am., 61, 3, 729-746, doi:10.1785/BSSA0610030729.

White, R. A. and W. L. Ellsworth (1993). Near source short to intermediate period ground motions, U. S. Geol. Surv. Prof. Pap., 1550C, C31-C46.

Woo, J. U., M. Kim, D. H. Sheen, T. S. Kang et al. (2019). An in-depth seismological analysis revealing a causal link between the 2017 M_W 5.5 Pohang earthquake and EGS project, J. Geophys. Res., Solid Earth, 124, 12, 13060-13078, doi:10.1029/2019JB018368.

Yerkes, R., P. Levine and C. Wentworth (1990). Abnormally high fluid pressures in the region of the Coalinga earthquake sequence and their significance, U. S. Geol. Surv. Prof. Pap., 1487, 235-257.

Yu, Y., W. L. Ellsworth and G. C. Beroza (2024) (submitted). Accuracy and Precision of Earthquake Location Programs: Insights from a Synthetic Controlled Experiment, Seimol. Res. Lett., SRL-D-24-00354.

Zoback, M. D., M. L. Zoback, V. S. Mount, J. Suppe et al. (1987). New evidence on the state of stress of the San Andreas fault system, Science, 238, 4830, 1105-1111, doi:10.1126/science.238.4830.1105.

***CORRESPONDING AUTHOR: Wiliam L. ELLSWORTH**,
Stanford University, Department of Geophysics, USA
e-mail: wellsworth@stanford.edu